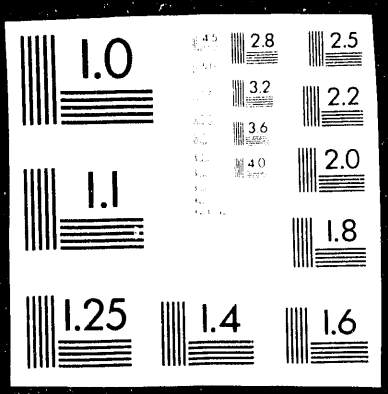

TABLE 1. - Characteristics of the 260-mD fired Berea sandstone sample from routine core analysis and mercury intrusion porosimetry

Air permeability, mD	260.0
Porosity, %	19.6
Total pore surface area, m^2/g	4.41

NIPER-581
(DE92001036)

Three-Phase Permeabilities and Other Characteristics of 260-mD Fired Berea

By
Dan Maloney
Alan Brinkmeyer

April 1992

Performed Under Cooperative Agreement No. DE-FC22-83FE60149

IIT Research Institute
National Institute for Petroleum and Energy Research
Bartlesville, Oklahoma

Bartlesville Project Office
U. S. DEPARTMENT OF ENERGY
Bartlesville, Oklahoma

NIPER-581
Distribution Category UC-122

Three-Phase Permeabilities and Other Characteristics of 260-mD Fired Berea

By
Dan Maloney
Alan Brinkmeyer

April 1992

Work Performed Under Cooperative Agreement No. DE-FC22-83FE60149

Prepared for
U.S. Department of Energy
Assistant Secretary for Fossil Energy

Rhonda L. Patterson, Project Manager
Bartlesville Project Office
P. O. Box 1398
Bartlesville, OK 74005

Prepared by
IIT Research Institute
National Institute for Petroleum and Energy Research
P. O. Box 2128
Bartlesville, OK 74005

TABLE OF CONTENTS

TABLES

ILLUSTRATIONS

ILLUSTRATIONS—Continued

Page

THREE-PHASE RELATIVE PERMEABILITIES AND OTHER CHARACTERISTICS OF 260-mD FIRED BEREA

by Dan Maloney and Alan Brinkmeyer

ABSTRACT

A laboratory investigation was conducted to determine relative permeabilities and other characteristics of a 260-mD fired Berea sandstone. The mineralogical and physical characteristics of the sample were characterized by XRD tests, thin section analyses, mercury injection tests, and centrifuge capillary pressure and wettability tests. Two-phase oil/water relative permeabilities were measured under several stress conditions. Resistivity characteristics of the sample were also evaluated during several of the oil/water tests. Oil/gas and gas/water relative permeabilities were measured during steady-state tests. Three-phase steady-state oil/gas/water tests were performed for six DDI saturation trajectories (decreasing brine and oil saturations, increasing gas saturation) in which the sample was not cleaned between saturation trajectories.

Oil/water relative permeability results for two different confining-stress conditions were similar. The relative permeability results for unstressed 260-mD Berea samples, however, were different than those of the stressed samples. Applying test results from unconfined core plugs toward studying specific reservoir processes should, therefore, be done with caution. Relative permeability and resistivity results measured during a waterflood test on the 260-mD rock did not agree with measurements from steady-state tests. Water retention at the outlet face of the rock, as shown by CT scans which were taken during the flood, probably contributed heavily toward the erroneous nature of the unsteady-state relative permeability results. These results show that particular care should be taken when evaluating laboratory resistivity and relative permeability results from tests in which saturation conditions are non-uniform.

Two- and three-phase relative permeabilities for each fluid phase were primarily affected by the saturation of that phase when the wetting phase (brine) was also present and for conditions of appreciable flow of all of the phases. Water relative permeability versus water saturation results were similar for both two-phase and three-phase flow systems. This result, which indicates that the wetting phase relative permeability is a unique function of the wetting phase saturation, agrees with the results from other investigations. Within the range of saturation conditions imposed during the laboratory tests, gas relative permeability versus gas saturation results were similar from two-phase gas-brine and three-phase gas-oil-brine tests. During these tests, gas relative permeabilities were primarily dependent upon gas saturations. However, lower oil saturations were achieved during three-phase tests compared to two-phase results. Oil saturations as low as 20% were achieved with oil flowing in the three-phase system whereas the residual oil saturations during two-phase oil/brine tests were approximately 37%. Since mobilization of the oil phase was possible at lower saturations in the three-phase system compared to the two-phase system, two-phase oil relative permeability data were inadequate for describing oil relative permeabilities at oil saturations close to and less than the two-phase residual oil saturation condition. With oil saturations greater than the two-phase residual oil condition, two- and three-phase oil relative permeability results were similar and the three-phase oil results tended to fall within the two-phase oil hysteresis envelopes.

INTRODUCTION

Multiphase flow is a common phenomenon in production from petroleum reservoirs. The initial or primary production from a reservoir may include gas, oil, brine, or combinations of the three. Later during the productive life of a reservoir, two-phase flow occurs as fluid such as brine is injected into a reservoir to boost production. Finally, if enhanced oil recovery techniques are used to maximize hydrocarbon recovery, multiphase flow processes are virtually guaranteed to occur. With multiphase flow, the fluids compete for the same flow paths through the reservoir rock. The additional resistance to flow is described by normalizing permeabilities for each of the flowing phases at each fluid saturation condition with respect to a base permeability. This measurement and normalization process yields relative permeability data.

The concept of relative permeability for two-phase flow is not new. Work on developing two-phase flow relationships probably began in 1859, and through the years techniques for using the results have been refined for estimating petroleum reservoir productivity and performance. Efforts to extend the techniques for three-phase flow began in 1941, but difficulties limited progress in this area. Three-phase flow experiments for determining relative permeability relationships are very difficult to perform. Keeping track of fluid saturations in a rock during three-phase steady-state flow experiments was virtually impossible until the recent advent of techniques to monitor in situ fluid saturations directly during flow experiments. Correlations have been developed to predict three-phase flow effects from two-phase flow measurements, but such correlations are not always correct or accurate. The primary reasons for the limited knowledge

with respect to three-phase flow systems are the scarcity of accurate three-phase relative permeability laboratory data and laboratory measurement systems.

NIPER has conducted DOE-funded relative permeability research for over 6 years. The objectives of this work have been to improve laboratory measurements of three-phase relative permeability so that reliable measurements are achieved, and to investigate the influences of rock, fluid, and rock/fluid properties on two- and three-phase relative permeabilities. This work has yielded improvements in measurement techniques and equipment including the development of an X-ray and microwave scanning instrument for monitoring fluid saturations during relative permeability experiments; the development of a high pressure coreholder that is semitransparent to microwaves; improvement in microwave technology for scanning rocks with thicknesses greater than 2.54 cm, and continual improvements in relative permeability measurement systems and techniques. NIPER's three-phase laboratory investigations have yielded interesting results.[1-8] Three-phase experiments with Berea sandstone to demonstrate viscous effects on relative permeability[3] showed that variations in permeabilities as a result of variations in rock characteristics could be seen even for samples cut from the same quarried block of rock; brine relative permeabilities are a function of the brine saturation; gas relative permeabilities are essentially functions of the gas saturation; oil relative permeabilities were functions of all three-saturations; and oil and water relative permeabilities were essentially independent of oil viscosity for viscosities in the 1 to 50 cP range. Water relative permeabilities decreased with increasing wetting phase viscosity. Test results were within reasonable repeatability considering hysteresis effects.

During FY89, NIPER investigated the effects of rock characteristics on relative permeabilities and compared the results of Berea and Bentheimer sandstone samples.[4] The two sandstones were almost identical except for the greater amount of very small (microporosity) and very large (megaporosity) pores for the Berea sandstone compared to the Bentheimer sandstone. Relative permeability results for the two sandstones were noticeably different, and these differences were attributed to the differences in pore size distributions. Comparison of oil-brine flow test results showed that residual oil saturations for the Bentheimer sample were lower than those of the Berea sample; the range of mobile saturations for the Bentheimer sample were broader; and that data from both samples were subject to hysteresis effects. Under three-phase flow conditions, water relative permeabilities for both samples were influenced by water saturations and not by oil or gas saturations. At equivalent water saturations, the water relative permeabilities for the Berea were less than those for the Bentheimer sample due to the influence of microporosity. Oil relative permeabilities under three-phase flow conditions were affected by all three-phase saturations for both samples. However, the Berea oil relative permeabilities were less affected by gas at low gas saturations since the Berea had greater megaporosity than the Bentheimer. The Bentheimer results formed a larger three-phase mobile saturation envelope than the Berea results.

Relative permeabilities and other characteristics of a 700-mD Berea sandstone were measured during FY90.[6] Hysteresis was evident in each multiple-cycle centrifuge capillary pressure experiment performed on the 700-mD Berea. The primary effect of the cycle-dependent hysteresis was a reduction in the wettability index with successive drainage and imbibition cycles. Hysteresis in relative permeability results for the water-wet rock was essentially limited to a shift in nonwetting phase relative permeability versus saturation curves between the first drainage and first imbibition tests in the direction of lower brine saturation for nonwetting phase saturations close to and less than the residual non-wetting phase saturation values. Two-phase measurements did not yield identical results. Mercury intrusion tests demonstrated that the porosimetry tests were useful for discerning differences in microporosities when characteristics of different samples are compared.

The FY91 research program was designed to build upon the previous results for the project with emphasis on obtaining data which can be used in developing three-phase relative permeability correlations and in describing the relationships among pore and grain size distributions and relative permeabilities.

EXPERIMENTAL PROCEDURES AND MEASUREMENTS

Sample Physical Characteristics

Berea sandstone was selected as the rock material for this investigation. Routine permeability and porosity experiments were conducted with plug samples from several blocks of Berea sandstone to find a sample with gas permeability in the 100 to 300 mD range. The 300-mD range was targeted to provide results for comparison with those of the higher-permeability Berea and Bentheimer sandstones previously characterized.[4, 6] A Berea sandstone block with a gas permeability of 270 mD and porosity of 19.6% was selected. The brine permeability of the sample was later measured as 260-mD, so for simplicity, the rock was designated as a 260-mD Berea sandstone. The new sample was selected to be similar to those samples with respect to mineralogy but slightly different with respect to porosity, permeability, and pore and grain shape, size, and number distribution characteristics.

The tests in this investigation were conducted on fired rock samples. Plugs and slabs of the Berea were cut from the block and were fired in an oven at 540° C for 24 hours to stabilize clay minerals. The 540° C firing temperature was 460° lower than the firing temperature that was used for samples tested in FY88, 89, and 90 project years. The lower firing temperature was selected as a compromise between the need for stabilizing clay minerals while at the same time preserving other rock properties. Firing at 1,000° C often leaves sandstone plugs with a refractory brick-like quality and can shatter some of the sandstone

grains if the temperature gradient changes abruptly during the heating and cooling processes.

Samples of the fired rock were subjected to routine core analysis, X-ray diffraction (XRD) analysis (bulk and clay minerals), thin section microscopic evaluation, and mercury intrusion porosimetry. Pore and grain size distributions for the fired rock were first characterized by petrographic image analysis (PIA). The PIA system consists of a Dage MTI camera mounted on a Nikon light microscope. Output from the camera is interfaced with a microcomputer. The microcomputer digitizes the images and performs various petrographic measurements and calculations. Features with dimensions in the sub-micron range were ignored in microscopic grain and pore size number distribution calculations because of microscopic resolution limitations. Five hundred pores and 500 grains were measured by evaluating thin sections with the aid of a petrosgrapic image analysis system. Mercury intrusion porosimetry tests were conducted to further characterize the rock's pore size distribution—particularly in the sub-micron size range. Volume and pressure measurements from tests in which mercury was forced into the rock pores at pressures from 3.45 kPa to 413 MPa were used to calculate pore diameters and mercury intrusion data.

Plugs of 2.5 cm diameter and 2.5 cm length were cut for mercury injection porosimetry tests. Plugs for relative permeability tests with confining pressure were of 3.8 cm diameter with lengths to 15 cm. A sample with 15.8 cm length and 1.9 cm by 5.1 cm rectangular cross section was prepared for steady-state relative permeability tests. Shallow grooves were cut in the sample along the sample ends and at positions 5 cm from each end. The grooves were painted with silver conducting paint, then a wrap of copper wire was placed in each groove. The copper wire was soldered into the groove to provide excellent electrical contact with the sample. The sample was encased in casting plastic (Castolite AP acrylic-polyester resin). Two pressure taps were installed along the top of the sample and were spaced 2.5 cm from the inlet and outlet rock faces. The pressure drop between the pressure taps and the gage pressure at the upstream pressure tap were measured using Rosemount pressure transmitters. Injection pressures during flow experiments with the plastic-encased sample were kept low — less than 2 atm gauge pressure — to avoid cracking the plastic and to minimize gas compressibility effects. A similar sample was prepared for resistivity measurements.

The tests described in this report were conducted at 25° C. Nitrogen was used as the gas phase in relative permeability measurements involving gas as one of the flowing phases. Unless noted otherwise, the test liquids were brine (1% by weight NaCl in water) and an isoparaffinic oil (Soltrol 100, a product of Phillips Petroleum Company). The interfacial tension between this brine and oil was 31 to 37 mN/m at 23° C. The oil phase was tagged with 10% by weight iodododecane for steady-state relative permeability tests in which water and oil phases were present. The brine phase was tagged with sodium iodide for gas/water steady-state tests, so that saturations could be accurately determined by both X-ray and microwave attenuation techniques. The terms brine and water are used synonymously within the context of this report.

Capillary Pressure Measurements

Oil/brine capillary pressure and wettability index characteristics were measured for two samples of the 260-mD Berea sandstone. The test fluids were mineral oil and 1% by weight NaCl brine. Measurements were recorded during drainage and imbibition experiments performed using a Beckman J-6M centrifuge at centrifuge speeds from 200 to 3,800 RPM, corresponding to oil-water capillary pressures from about 0.1 to 17 psi. Capillary pressure data were measured during first drainage, first imbibition, and second drainage saturation cycles to provide information on both capillary pressure and wettability characteristics. The capillary pressure-saturation relationships were determined using the Rajan[9] method. Wettability indices were calculated using the USBM technique.[10]

Relative Permeability Measurements

Unsteady-State Tests

Several unsteady-state oil/water relative permeability tests were conducted on similar samples of fired Berea. Injection fluids consisted of 1.01 cP brine (2% NaCl by weight in deionized water) and mineral oil of 23.5 cP viscosity. Tests were conducted with the core plugs subjected to 500 psig confining pressure. After measuring the brine permeability, each sample was flooded with oil to the residual brine saturation test condition. Unsteady-state measurements were recorded as the test plugs were subsequently flooded with brine (imbibition cycle for a water-wet rock). The JBN[11] method was used to calculate oil and brine permeabilities. Permeabilities were normalized with respect to the permeabilities of the samples to brine under conditions of complete brine saturation.

A number of additional oil/brine unsteady-state relative permeability tests were performed on a sample of 260-mD Berea sandstone to evaluate the suitability of a waterflooding test design criteria that was listed in the literature ($Q\mu L \geq 1 - 5$).[12] These tests were performed to check whether better agreement could be obtained among unsteady- and steady-state relative permeability measurements when certain experimental criteria were honored.

Waterflood Test with Resistivity and CT Saturation Measurements

One waterflood experiment was performed on a sample of the 260-mD Berea sandstone in which the electrical properties and saturation distributions were measured during the test.

The sample was 16 cm long and had a 2 cm by 5 cm rectangular cross-section. The dry rock was outfitted with

five electrodes which were equally spaced along the length of the sample. The electrodes were attached for measuring the electrical resistances across different segments of the sample. The four-electrode technique (segregation of current and potential electrodes) was used for resistance measurements. The rock was jacketed in an acrylic polyester resin for fluid flow confinement.

The dry, epoxy-jacketed sample was placed in a container which minimized the effects of X-ray beam-hardening on the CT scan results. The container was set on an X-ray scanning table and was scanned longitudinally using an 8 mm wide X-ray beam at a 125 KV power level. The rock was then vacuum saturated with a 7.7% by weight KI brine. A scan was taken of the brine-saturated rock. The iodine component of the brine mixture acted as a tagging agent to increase the X-ray attenuation characteristics of the brine phase, thereby allowing better resolution between the brine and oil phases in the rock. The dry CT scans, brine-saturated CT scans, and the CT attenuation numbers for the brine and oil were sufficient for the calibration of the CT for two-phase brine/oil saturation determination as described in a quarterly report for this project.[13]

Electrical resistance was measured across each combination of the five electrodes at 100% brine saturation. The core was then oil-flooded to an irreducible brine saturation condition using a mineral oil of 22 cP viscosity. A 40 mL/hr waterflood was conducted on the rock. Resistance measurements and CT scans were recorded with each measurement of the effluent oil and brine volumes.

CT saturations for each rock section were determined by averaging the values of all voxels across the relevant section of the CT scan image. The CT image of the 100% brine-saturated rock required correction because of excessive attenuation. The longitudinal orientation of the rock within the CT gantry caused greater X-ray attenuation than was expected, especially when the rock was saturated with tagged brine. Results for the 100% brine-saturated rock were therefore calculated from dry scan, porosity, and fluid attenuation measurements. The correction method assumed a uniform porosity for each voxel of the CT image. This assumption of uniform porosity is a limiting factor for CT saturation determination but is not a bad approximation for this homogeneous rock.

Steady-State Tests with Confining Pressure

A two-phase steady-state oil/water relative permeability test was conducted on a plug of the 260-mD Berea under conditions of 3,200 psig confining pressure. This test was conducted to provide data to compare unconfined sample permeability results with those of a confined sample. The 1.6 cP brine consisted of 6% NaCl and 6% NaI by weight in deionized water. The oil was a 1 cP viscosity refined oil (Soltrol 100). The plug was initially saturated with brine and was then placed in a coreholder. Changes in pore volume were measured as the confining pressure on the sample was increased to 3,200 psig. Steady-state measurements were recorded as brine and oil were simultaneously injected into the rock for two drainage and one imbibition saturation cycles. X-ray absorption techniques were used to monitor fluid saturations within the rock during the test. The NaI in the brine served as an X-ray tag. X-ray and microwave attenuation techniques for determining saturations are described in appendix A.

Steady-State Tests on the Unconfined Plastic-Encased Sample

Two-phase and three-phase steady-state oil/water, gas/water, gas/oil, and oil/gas/water relative permeability tests were conducted on the unconfined plastic-encased sample. Between tests, the rock was cleaned with isopropyl alcohol and pentane and dried with nitrogen gas.

The test fluids used for the two-phase oil/brine test were deionized water containing 1% by weight NaCl as the brine phase and Soltrol 100 (an isoparaffinic oil available from Phillips Petroleum Co.) tagged with 10% by weight iodododecane as the oil phase. A new technique was used to calibrate the X-ray for saturation measurements. Scans of the rock when saturated with 1% NaCl brine served as the calibration data for the condition of complete brine saturation. Additional scans were taken after the rock was flooded with a tagged brine which had the same X-ray absorption characteristics as the tagged oil. Thus, X-ray calibrations were developed without saturating the rock with oil and without having to interpret fluid saturation distributions within the rock from volumetric measurements. Untagged brine was flooded through the rock to remove all traces of the tagged brine in preparation for the steady-state relative permeability test. The rock was oil-flooded to residual brine saturation conditions, then two-phase measurements were recorded for an imbibition (i1) and a second drainage (d2) saturation cycle. The microwave scanner was also used to monitor fluid saturations.

After cleaning, the rock was saturated with oil and a steady-state gas/oil test was conducted. Nitrogen gas was used as the gas phase. The rock was cleaned after the gas/oil test. The rock was saturated with brine. Steady-state gas/brine measurements were recorded for two drainage saturation cycles and one imbibition cycle.

Three-phase steady-state relative permeability tests were initiated on the sample upon completing the two-phase tests. Measurements were recorded during six DDI saturation trajectories (decreasing brine and oil saturations, increasing gas saturation). After completing a saturation trajectory, the plug was waterflooded to residual gas and oil saturation conditions. A new saturation trajectory was started by establishing brine and oil flow at a target brine fractional flow ratio before injecting gas into the rock. The target brine fractional flow ratios were selected to provide a spread of three-phase results. Initial oil and brine injection rates were adjusted to yield a pressure drop across the length of the sample that was equal to approximately half of the range of the differential pressure transmitter. The first gas rate was adjusted to yield a pressure drop across the rock sample equal to approximately 80% of the differential pressure transmitter range. Permeabilities were calculated from flow rate and pressure drop measurements

while saturation distributions were calculated from X-ray and microwave scans. Saturation changes along the same saturation trajectory were established by either doubling the gas rate or halving the oil and brine rates, depending upon whether the pressure drop across the plug was closer to 50% or 80% of full scale. This technique of halving the liquid injection rates or doubling the gas rate was described by Oak et al.[18] Additional measurements were recorded after doubling the gas rate or halving the oil and brine rates until either the brine and oil saturations were diminished to residual values or until the oil or brine injection rates were too low for practical measurement. Microwave and X-ray attenuation techniques that were used to determine saturation distributions within the rock during the steady-state tests are described in appendix A. An alternative method for determining three-phase saturations from X-ray results is described in appendix B.

RESULTS

Sample Physical Characteristics

Routine core analysis and mercury intrusion porosimetry results are given in Table 1. The permeability and porosity of a plug of the fired rock were 260-mD and 19.6%, respectively. XRD results indicate that the rock consists of 92% quartz, 5% feldspar (of which half is plagioclase feldspar), 1% dolomite, and 2% illite.

Evaluations of thin sections of the rock showed that the sandstone grain and pore size distributions by number percent for features greater in size than 10 μm are fairly well represented with log-normal distribution functions, as shown in Fig. 1. Note that the y-axis on the figure is a log scale while the x-axis is a normal probability scale. Table 2 presents sizes corresponding to 84, 50, and 16 percentile values as well as σ results where

$$\ln \sigma = 0.5 \ln \left(\frac{d_{84}}{d_{16}}\right) \qquad (1)$$

Mercury porosimetry results for the sandstone indicate that the median pore diameter by volume is 9.56 μm. Mercury intrusion results for the sample are shown in Fig. 2, which is a plot of log specific differential intrusion volume versus pore diameter. Figure 2 indicates that the sample contains a significant volume of pores of size less than 10 microns.

Centrifuge Capillary Pressure Tests

Figure 3 shows oil/brine capillary pressure results for two samples of the 260-mD Berea sandstone. The test results were similar for brine saturation fractions to 0.35 and were almost identical for saturation fractions greater than 0.35. USBM wettability indices for the two samples were 1.32 and 1.35, indicating that the rock is strongly water-wet.

Relative Permeability Measurements

Unsteady-State Tests

The porosity of the first test plug under ambient pressure conditions was 19.3% and dropped to 18.3% as the confining pressure was increased to 500 psig. The brine permeability of the plug was 157-mD. Relative permeability results for three imbibition cycles are shown in Fig. 4. The relative permeability versus saturation results for the three imbibition cycles followed the same trends. Hysteresis effects did not appear to be significant in the test results. Figure 5 shows unsteady-state relative permeabilities measured on a second plug of similar permeability. Injection rates of 25, 50, and 400 mL/hr yielded similar oil relative permeability results while the water relative permeability curves shifted in the direction of higher relative permeability with increasing injection rate. Collectively, though, the unsteady-state results in Figs. 4 and 5 for two different plugs are similar. Figure 6 shows the ratios of water to oil relative permeabilities from the multiple rate test plotted against normalized brine saturations. The trend of the data on Fig. 6 suggests that errors in residual saturation measurements may have contributed to the discrepancies among water results from the multiple rate test. Figure 7 shows steady-state results for a sample confined under a higher stress state. The unsteady-state results from Figs. 4 and 5 are similar to those from the steady-state test on Fig. 7. The steady-state results cover a broader range of water saturations, however.

Waterflood Test with Resistivity and CT Saturation Measurements

Average saturations from volumetric and CT measurements were in suitable agreement considering the resolution of the CT scanner. Figure 8 is a comparison of the volumetric and CT brine saturations during the waterflood test. Table 3 contains pertinent data associated with each flood profile.

Figure 9 shows brine saturation profiles as the unsteady-state waterflood progressed. Plot 9A shows the saturation profile at the end of the oil flood in which the water saturation was at a residual condition. Flood profiles B and C show the brine front moving through the rock. Water breakthrough occurs on profile plot D. Plots E through H show saturation distributions within the center of the sample at several time intervals during the waterflood.

Figure 10 log-log plots show changes in resistivity indices with water saturation for regions of the rock between electrodes 1-2, 2-3, 3-4, and 4-5. Electrode 1 was at the outlet end of the rock while electrode 5 was at the inlet end of the sample. The positions of the other electrodes are shown in Fig. 9 as solid lines. Although the brine saturation distributions between the resistivity electrodes in profiles E through H in Fig. 9 appear to be uniform and stable, the resistivity indices shown in Fig. 10 continued to vary toward the "straight line" fit between

the 100% water and residual water saturation data as the flood progressed. Resistivity index versus saturation trends often appear as straight lines on log-log plots (for examples, check references 14 and 15). Figures 9 and 10 results suggest that the CT scanner did not have the resolution necessary to determine brine saturations to the level that effects the flow of electrical current through the pore spaces, or that saturation data from a vertical plane through the center of the sample were insufficient for characterizing the saturations in the bulk of the sample. This is particularly apparent for the resistivity index between electrodes 4-5 at the inlet end of the rock.

Figure 11 shows unsteady-state oil/water relative permeability results calculated from pressure drop and production measurements recorded during the waterflood test. The data were normalized with respect to the oil permeability of 120-mD at a residual water saturation fraction of 0.274. The results clearly appear to be in error considering the differences among these results and those of Figs. 4, 5, and 7. The water saturation distributions in Fig. 8 show that high water saturations were retained at the outlet face of the rock throughout the flood, indicative of capillary end effects. The actual water saturations at the outlet face from Fig. 9 do not correspond with the water saturations for data sets in Fig. 11, which were calculated by the JBN unsteady-state method. Water retention at the outlet face of the rock probably contributed heavily toward the erroneous nature of these unsteady-state relative permeability results.

This waterflood/CT/resistivity experiment served as a trial test to establish procedures for measuring saturations using the CT scanner during resistivity tests. Perhaps the most interesting finding in this test was the relationship between the resistivity index across adjacent electrodes and the brine saturation between these electrodes as the waterflood progressed. Similar trends were shown by Sprunt et al.[15] A more in-depth look at the relationship between non-uniform saturation distributions and resistivity measurements may be continued next year.

Steady-State Test with Confining Pressure

The porosity of the plug was 19.3% unconfined and dropped to 18.3% when the confining pressure was increased to 3,200 psig. The permeability of the brine-saturated sample was 260-mD. Oil and brine permeabilities were normalized with respect to the permeability of the brine-saturated rock. Steady-state relative permeability results are shown in Fig. 7. Little saturation-history-dependent hysteresis was seen in the data after the first drainage cycle.

Steady-State Tests on the Unconfined Plastic-Encased Sample

Oil/water relative permeability results for the sample are provided in Table 4 and are shown in Fig. 12. The permeability values were normalized with respect to the brine permeability of the sample when the sample was completely saturated with brine (260-mD). The brine relative permeability curves followed the same trend for both saturation cycles, whereas lower oil relative permeabilities resulted at intermediate saturations during the second drainage cycle. Resistivity measurements were also recorded during the test using the 2-electrode method in which the electrodes were centered 5.1 cm apart along the length of the 15.8-cm-long sample. Resistivity index results are shown in Fig. 13. The saturation exponent calculated from the imbibition data was 2.2 compared to the 2.4 result from the drainage data. Viewed collectively, the imbibition and drainage resistivity data follow the same trend. This is consistent with the brine relative permeability results. The saturation exponent for the combined imbibition and drainage data is 2.2. Note that the resistivity trends in Fig. 10 for conditions of residual water and complete water saturations (first two points on each graph) are similar to those of Fig. 13.

The limited results from the gas/oil steady-state test are given in Table 5 and are shown in Fig. 14. The results are for conditions in which no residual water saturation was present. The quality of the gas/oil data is suspect. Gas/water two-phase results are listed in Table 6 and are presented in Fig. 15. The gas relative permeability curves were similar for the two drainage cycles, while the imbibition results were significantly different. Toward the end of the imbibition cycle as the brine permeability at residual gas saturation conditions was measured, the brine permeability dropped, suggesting fines migration. The flow direction was reversed, restoring the permeability. The forward flow direction was resumed for the second drainage cycle. The gas relative permeability curves for the two drainage cycles are similar, as are the brine relative permeabilities on the first drainage and imbibition curves. Other discrepancies in the data may be related to cycle dependent hysteresis, sample plugging, or the temporary change in flow directions. Further tests to examine the causes of the discrepancies were not possible because of time limitations.

The saturation trajectories that were achieved during the three-phase steady-state test are shown in Fig. 16. Three-phase water relative permeability results are provided in Table 7. Two- and three-phase water relative permeabilities are shown in Fig. 17. The two-phase and three-phase water relative permeabilities follow the same trend, indicating that the water relative permeabilities for the sample under both two- and three-phase flow conditions are primarily influenced by the water saturation conditions of the sample. Two- and three-phase oil results are plotted in Fig. 18. The two- and three-phase oil relative permeabilities also followed similar trends, indicating that for this rock, the oil relative permeabilities in multiphase systems were primarily affected by oil saturations. Two- and three-phase gas relative permeabilities are plotted in Fig. 19. The two-phase gas results in Fig. 19 are for the first imbibition and second drainage tests in which the greatest differences in gas results occurred. The three-phase gas results fell within an envelope defined by these two-phase results.

DISCUSSION

Most of the relative permeability results in this report were normalized with respect to the water permeability under conditions of complete water saturation. Previous results from this project were normalized with respect to the oil permeability from two-phase oil/water tests at residual water saturation conditions. The change in normalization procedures was made to provide consistency with the methods of other investigators.

The relative permeability curves for confined and unconfined samples of the same rock were not identical. Results for samples confined at 500 psig and 3,200 psig were similar, suggesting that the application of some confining pressure is better than testing unconfined samples when test results must be related to reservoir processes in which high net confining pressures are present. Changes in pore dimensions and closure of microfractures with stress as demonstrated by the characteristic decrease in pore volume with stress that most rocks exhibit are probably responsible for much of the differences in unconfined and confined test results. However, the comparisons of two- and three-phase relative permeabilities in this report for unconfined samples are still considered valid as both types of tests were conducted under the same net confining stress conditions. Since thin sections are cut from unconfined rock samples, comparisons of pore size distributions from thin sections with permeability results are most applicable for rock samples that are tested in the unconfined state.

The rock was not cleaned after each DDI saturation cycle during the three-phase tests. Instead, the rock was flooded with brine to drive the oil and gas saturations to residual conditions before starting a new saturation trajectory. Two- and three-phase relative permeabilities for a fluid phase were primarily affected by the saturation of that phase for tests in which the wetting phase (water) was also present. Two- and three-phase results for a particular phase with respect to the saturation of that phase were similar when the wetting phase was one of the phases present in the rock, considering hysteresis. This result is in agreement with those of Leverett and Lewis[20] for conditions of appreciable flow of all three-phases. Three-phase results for each phase tended to fall within the two-phase hysteresis envelope. However, lower oil saturations were achieved during three-phase tests compared to two-phase results. Oil saturations as low as 20% were achieved with oil flowing in the three-phase system whereas the residual oil saturations during two-phase oil/brine tests were approximately 37%. Since mobilization of the oil phase was possible at lower saturations in the three-phase system compared to the two-phase system, two-phase oil relative permeability data were inadequate for describing oil relative permeabilities at oil saturations close to and less than the two-phase residual oil saturation condition. With oil saturations greater than the two-phase residual oil condition, two- and three-phase oil relative permeability results were similar and the three-phase oil results tended to fall within the two-phase oil hysteresis envelope. References 16 through 20 provide three-phase results from some other investigations for comparison.

The results from the CT/resistivity/waterflood test suggest that particular care should be taken when evaluating resistivity or relative permeability data for rocks containing non-uniform saturation distributions.

CONCLUSIONS

Some conclusions from this work are as follows:

1. This 260-mD fired Berea sandstone was strongly water-wet. USBM wettability indices from oil/water centrifuge test measurements were close to 1.
2. Unsteady-state and steady-state oil/water relative permeability results for the rock were similar when the rock was tested with confining pressure for confining pressures in the 500 to 3,200 psig range. The relative permeability curves for confined and unconfined samples of the same rock were not identical, suggesting that care should be taken when applying test results from unconfined core plugs toward studying reservoir processes. However, the comparisons of two- and three-phase relative permeabilities in this report for unconfined samples are still considered valid as both types of tests were conducted under the same net confining stress conditions.
3. Particular care should be taken when evaluating resistivity and relative permeability results from tests in which saturation conditions are non-uniform. The relative permeability and resistivity results measured during a waterflood test on the 260-mD rock did not agree with measurements from steady-state tests. Water retention at the outlet face of the rock, as shown by CT scans which were taken during the flood, probably contributed heavily toward the erroneous nature of the unsteady-state relative permeability results. Further investigation into relationships between resistivities and non-uniform saturation distributions is required.
4. Water relative permeability versus water saturation results were similar for both two-phase and three-phase flow systems. This result, which indicates that the wetting phase relative permeability is a unique function of the wetting phase saturation agrees with the results from other investigations.
5. Within the range of saturation conditions imposed during the laboratory tests and when the wetting phase (water) was also present in the system, two- and three-phase oil relative permeabilities were primarily dependent upon oil saturations while gas results were primarily dependent upon gas saturations. Three-phase results for each phase tended to fall within the hysteresis envelope from two-phase results.
6. Lower residual saturation conditions than those achieved at the end of two-phase processes resulted during the three-phase tests. Oil saturations as low as 20% were achieved with oil flowing in the three-phase system whereas the residual oil saturations during two-phase tests were approximately 37%.

7. The three-phase saturation envelope or range in saturations with three flowing phases for the 260-mD Berea sample was relatively small.

ACKNOWLEDGMENTS

This work was performed for the U. S. Department of Energy (DOE) under Cooperative Agreement DE-FC22-83FE60149. The authors thank Willis Waldorf, Ron Masias, Mike Crocker, and Liviu Tomutsa, all of NIPER, for their assistance in the laboratory with steady-state relative permeability, centrifuge capillary pressure, and CT scan measurements. Appreciation is also extended to Eddie Lou, who worked on the project during the summer under an AWU Scholarship, for conducting unsteady-state relative permeability tests and to Jesus Betancourt of INTEVEP for his valuable contributions in the development of unsteady-state relative permeability and centrifuge capillary pressure computer programs to facilitate data analysis. Finally, we thank the NIPER management and personnel who reviewed this manuscript, and Rhonda Patterson, the DOE Project Manager, for her support.

REFERENCES

1. Parmeswar, R., and N. Maerefat. *A Comparison of Methods for the Presentation of Three-Phase Relative Permeability Data*. Proc. of the Soc. Pet. Eng. 56th California Regional Meeting, Oakland, (April 2-4, 1986), pp. 151-157.

2. Parmeswar, R., N. Maerefat, and A. Brinkmeyer. *Preliminary Results on the Effect of Fluid Viscosity on Three-Phase Relative Permeability*. DOE Report NIPER-296, 1987.

3. Maloney, D., S. Mahmood, and M. Honarpour. *The Effects of Viscous Forces on Three-Phase Relative Permeability*. DOE Report NIPER-392, 1989.

4. Maloney, D., M. Honarpour, and A. Brinkmeyer. *The Effects of Rock Characteristics on Relative Permeability*. DOE Report NIPER-441, 1990 (NTIS Order NO. DE9000212).

5. Honarpour, M. and S. Mahmood. Relative Permeability Measurements: An Overview. SPE Tech. Today Series, *J. Pet. Tech.*, August, 1988.

6. Maloney, D., A. Brinkmeyer, and M. Honarpour. *Relative Permeabilities and Other Characteristics of 700-Millidarcy, Fired Berea Sandstone*. DOE Report NIPER-496, October, 1990.

7. Honarpour, M., D. Maloney, S. Suzuki, and L. Tomutsa. *Investigation of Cycle Dependent Centrifuge Capillary Pressure and Wettability Index Behavior for Water-wet High Permeability Sandstones*. Paper SCA 9006 Pres. at the Fourth Annual SCA Technical Conference, Dallas, TX, August 15-16, 1990.

8. Honarpour, M. and D. Maloney. *Relative Permeability Technology and Applications*. Paper SCA 9008 Pres. at the 4th Annual SCA Tech. Conf., Dallas, TX, Aug. 15-16, 1990.

9. Rajan, R.. *Theoretically Correct Analytical Solution for Calculating Capillary Pressure-Saturation From Centrifuge Experiments*. Paper J. Pres. at the SPWLA 27th Annual Logging Symposium, June, 1986.

10. Donaldson, E. and P. Lorenz. Wettability Determination and Its Effect on Recovery Efficiency. *SPEJ*, March, 1969, pp. 13-20.

11. Johnson, E., D. Bossler, and V. Naumann. Calculation of Relative Permeability from Displacement Experiments. *Trans. AIME*, December, 1958.

12. Batycky, J., F. McCaffery, P. Hodgins, and D. Fisher. Interpreting Relative Permeability and Wettability From Unsteady-State Displacement Measurements. *SPEJ*, June, 1981, pp. 296-308.

13. Maloney, D. *Quarterly Technical Report for April 1 - June 30, 1991. Volume II, Energy Production Research*. DOE Report NIPER-545, .

14. Lyle, W. and W. Mills. Effect of Nonuniform Core Saturation on Laboratory Determination of the Archie Saturation Exponent, *SPEFE* , March 1989.

15. Sprunt, E., K. Desal, M. Coles, R. Davis, E. Muegge. "CT-scan-Monitored Electrical Resistivity Measurements Show Problems Achieving Homogeneous Saturation", *SPE Formation Evaluation*, June 1991, p. 134-140

16. Oak, M., L. Baker, and D. Thomas. *Three-Phase Relative Permeability of Berea Sandstone*. Paper SPE/DOE 17370 Pres. at the SPE/DOE Enhanced Oil Recovery Symposium, Tulsa, OK, April 17-20, 1988.

17. Oak, M., and R. Ehrlich. A New X-ray Absorption Method for Measurement of Three-Phase Relative Permeability. *SPE Reservoir Engineering*, February, 1988, pp. 199-206.

18. Oak, M.. *Three-Phase Relative Permeability of Berea Sandstone*. Paper SPE/DOE 20183 Pres. at the SPE/DOE 7th Symposium on Enhanced Oil Recovery, Tulsa, OK April 22-25, 1990.

19. Dria, D., G. Pope and K. Sepehrnoori. *Three-Phase Gas/Oil/Brine Relative Permeabilities Measured Under Carbon Dioxide Flooding Conditions*. Paper SPE/DOE 20184 Pres. at the DOE/SPE 7th Symposium on Enhanced Oil Recovery, Tulsa, OK, April 22-25, 1990.

20. Leverett, M. and W. Lewis. Steady Flow of Gas-Oil-Water Mixtures Through Unconsolidated Sands. *Trans. AIME*, 1941, pp. 107 - 116.

TABLE 1. - Characteristics of the 260-mD fired Berea sandstone sample from routine core analysis and mercury intrusion porosimetry

Air permeability, mD	260.0
Porosity, %	19.6
Total pore surface area, m^2/g	4.41
Median pore diameter (by volume), μm	9.56

TABLE 2. - Log-normal distribution function characteristics for 260-mD fired Berea sandstone

Feature	d_{84}[1], μm	d_{50}, μm	d_{16}, μm	σ^2
Grains	205	139	93	1.485
Pores	143	84	51	1.674

1. 84% of the grains (by number) are smaller than the d_{84}.
2. $\ln\sigma = 0.5 \ln(d_{84}/d_{16})$.

TABLE 3. - Injection and saturation data recorded during an unsteady-state waterflood test using 260 mD Berea sandstone

Data Set	PV Injected	S_w Vol.	S_w CT	S_w - CT Electrode 1-2	S_w - CT Electrode 2-3	S_w - CT Electrode 3-4	S_w - CT Electrode 4-5
A	0.00	0.274	0.286	0.331	0.267	0.249	0.232
B	0.24	0.332	0.329	0.330	0.269	0.247	0.442
C	0.38	0.446	0.452	0.312	0.396	0.505	0.540
D	0.55	0.595	0.594	0.594	0.575	0.585	0.618
E	0.60	0.604	0.607	0.612	0.585	0.599	0.629
F	0.77	0.616	0.625	0.644	0.601	0.609	0.643
G	1.10	0.619	0.617	0.637	0.596	0.602	0.632
H	2.80	0.622	0.620	0.639	0.598	0.604	0.634

TABLE 4. - 260-mD Berea oil/water steady-state relative permeability results normalized with respect to k_w = 260 mD at S_w = 1.0

k_w, mD	k_o, mD	k_{rw}	k_{ro}	R_t/R_o	S_w	
275.66	0.00	1.052E+00	0.000E+00	1.00	1.000	i1*
0.00	181.00	0.000E+00	6.962E-01	9.22	0.339	
2.38	107.90	9.154E-03	4.150E-01	6.60	0.459	
3.75	65.70	1.442E-02	2.527E-01	5.00	0.475	
5.28	43.60	2.031E-02	1.677E-01	4.20	0.534	
7.98	6.25	3.069E-02	2.404E-02	3.11	0.570	
9.91	1.30	3.812E-02	5.000E-03	2.59	0.568	
10.20	0.00	3.923E-02	0.000E+00	2.76	0.629	
9.95	0.25	3.827E-02	9.615E-04	2.56	0.637	d2
9.76	1.29	3.754E-02	4.962E-03	2.65	0.620	
8.37	6.13	3.219E-02	2.358E-02	3.01	0.617	
6.19	16.40	2.381E-02	6.308E-02	3.51	0.561	
3.50	34.60	1.346E-02	1.331E-01	4.43	0.519	
3.10	54.90	1.192E-02	2.112E-01	5.04	0.480	
2.30	69.20	8.846E-03	2.662E-01	5.57	0.458	
0.00	128.60	0.000E+00	4.946E-01	7.78	0.407	

*Saturation cycle, i = imbibition, d = drainage

Resistivity results: i1, $R_t/R_o = 0.99\ (S_w^{-2.15})$; R = 0.97

d2, $R_t/R_o = 0.88\ (S_w^{-2.20})$; R = 0.99

TABLE 5. - 260-mD Berea gas/oil steady-state results normalized with respect to k_w = 260 mD at S_w = 1.0

k_g, mD	k_o, mD	k_{rg}	k_{ro}	S_o	S_g
234.0	0.0	8.999E-01	0.000E+00	0.000	1.000
0.0	183.4	0.000E+00	7.054E-01	1.000	0.000
136.0	0.0	5.231E-01	0.000E+00	0.409	0.591
37.9	38.8	1.458E-01	1.492E-01	0.528	0.472
19.9	45.1	7.654E-02	1.735E-01	0.618	0.382
8.2	77.2	3.154E-02	2.969E-01	0.841	0.159
2.3	106.1	8.846E-03	4.081E-01	0.929	0.071
0.184	192.5	7.077E-04	7.404E-01	0.997	0.003
0.0	225.7	0.000E+00	8.681E-01	0.998	0.002

TABLE 6. - 260-mD Berea gas/water steady-state results normalized with respect to k_w = 260-mD at S_w = 1.0

k_w, mD	k_g, mD	k_{rw}	k_{rg}	S_w	
0	260	0.000E+00	1.000E+00	0.000	d1*
260	0	1.000E+00	0.000E+00	1.000	
114.3	4	4.396E-01	1.538E-02	0.942	
80	21.6	3.077E-01	8.308E-02	0.890	
34.5	58.7	1.327E-01	2.258E-01	0.764	
22.77	77.4	8.758E-02	2.977E-01	0.709	
12.1	90.3	4.654E-02	3.473E-01	0.642	
2.27	134.9	8.731E-03	5.188E-01	0.547	
0	174.8	0.000E+00	6.723E-01	0.439	
2.5	138.9	9.615E-03	5.342E-01	0.517	i1
3.6	97.8	1.385E-02	3.762E-01	0.556	
9.2	58.6	3.538E-02	2.254E-01	0.593	
14.2	42.9	5.462E-02	1.650E-01	0.635	
16.8	26.4	6.462E-02	1.015E-01	0.671	
21.97	5.45	8.450E-02	2.096E-02	0.725	
33.5	0.785	1.288E-01	3.019E-03	0.775	
66.5	0.0	2.558E-01	0.000E+00	0.867	
57.1	2.64	2.196E-01	1.015E-02	0.896	d2
22.5	35.8	8.654E-02	1.377E-01	0.766	
9.0	61.8	3.462E-02	2.377E-01	0.698	
2.0	108.3	7.692E-03	4.165E-01	0.612	
0.0	151.3	0.000E+00	5.819E-01	0.538	

*Saturation cycle, i = imbibition, d = drainage.

TABLE 7. - Three-phase steady-state gas/oil/brine results normalized with respect to k_w = 260-mD when S_w = 1.0

k_g, mD	k_w, mD	k_o	k_{rg}	k_{rw}	k_{ro}	S_g	S_w	S_o	
0.05	7.2	0.375	1.923E-04	2.769E-02	1.442E-03	0.090	0.608	0.302	T1*
0.288	6.66	0.211	1.108E-03	2.562E-02	8.115E-04	0.119	0.600	0.281	
0.53	5.4	0.22	2.038E-03	2.077E-02	8.462E-04	0.107	0.613	0.280	
1.39	4.6	0.07	5.346E-03	1.769E-02	2.692E-04	0.163	0.592	0.245	
1.54	4.6	0.092	5.923E-03	1.769E-02	3.538E-04	0.194	0.590	0.216	
2.177	3.72	0.087	8.373E-03	1.431E-02	3.346E-04	0.223	0.571	0.206	
8.62	3.09	0.052	3.315E-02	1.188E-02	2.000E-04	0.271	0.521	0.208	
0.726	3.22	1.24	2.792E-03	1.238E-02	4.769E-03	0.117	0.526	0.357	T2
1.28	2.19	0.71	4.923E-03	8.423E-03	2.731E-03	0.186	0.492	0.322	
2.48	2.28	0.71	9.538E-03	8.769E-03	2.731E-03	0.200	0.483	0.317	
4.56	1.55	0.33	1.754E-02	5.962E-03	1.269E-03	0.220	0.458	0.321	
8.95	1.51	0.32	3.442E-02	5.808E-03	1.231E-03	0.221	0.463	0.317	
19.2	0.63	0.3195	7.385E-02	2.404E-03	1.229E-03	0.280	0.425	0.294	
0.16	0.98	3.39	6.154E-04	3.758E-03	1.304E-02	0.147	0.493	0.360	T3
0.47	0.72	1.71	1.808E-03	2.769E-03	6.577E-03	0.210	0.437	0.353	
1.32	0.78	1.74	5.077E-03	3.000E-03	6.692E-03	0.239	0.438	0.323	
2.47	0.74	1.69	9.500E-03	2.846E-03	6.500E-03	0.202	0.441	0.357	
5.169	0.734	1.68	1.988E-02	2.823E-03	6.462E-03	0.175	0.435	0.390	
11.75	0.64	1.55	4.519E-02	2.453E-03	5.962E-03	0.229	0.420	0.351	
0.42	6.7	0.61	1.615E-03	2.577E-02	2.346E-03	0.056	0.587	0.357	T4
0.71	4.4	0.356	2.731E-03	1.692E-02	1.369E-03	0.090	0.552	0.358	
1.38	3.86	0.244	5.308E-03	1.485E-02	9.385E-04	0.092	0.556	0.352	
2.94	2.85	0.22	1.131E-02	1.096E-02	8.462E-04	0.161	0.520	0.319	
5.1	2.55	0.169	1.962E-02	9.808E-03	6.500E-04	0.154	0.524	0.322	
9.1	2.27	0.167	3.500E-02	8.731E-03	6.423E-04	0.186	0.478	0.336	
14.34	1.95	0.158	5.515E-02	7.500E-03	6.077E-04	0.216	0.464	0.321	
0.75	0.46	7.36	2.885E-03	1.769E-03	2.831E-02	0.109	0.419	0.471	T5
1.16	0.39	4.78	4.462E-03	1.500E-03	1.838E-02	0.125	0.432	0.443	
2.2	0.37	4.64	8.462E-03	1.423E-03	1.785E-02	0.147	0.427	0.426	
4.9	0.16	4.74	1.885E-02	6.154E-04	1.823E-02	0.163	0.388	0.449	
8.54	0.38	3.35	3.285E-02	1.454E-03	1.288E-02	0.205	0.400	0.394	
16.7	0.2	3.3	6.423E-02	7.692E-04	1.269E-02	0.220	0.392	0.388	
21.9	0.18	3.18	8.423E-02	6.923E-04	1.223E-02	0.231	0.369	0.399	
0.21	2.16	1.81	8.077E-04	8.308E-03	6.962E-03	0.079	0.484	0.437	T6
0.51	1.6	1.44	1.962E-03	6.154E-03	5.538E-03	0.089	0.475	0.436	
0.57	1.35	1.62	2.192E-03	5.192E-03	6.231E-03	0.088	0.485	0.427	
1.13	1.13	0.96	4.346E-03	4.346E-03	3.692E-03	0.144	0.461	0.395	
2.5	1.16	0.95	9.615E-03	4.462E-03	3.654E-03	0.151	0.462	0.387	
5.75	1.42	0.95	2.212E-02	5.462E-03	3.654E-03	0.166	0.470	0.363	
9.9	1.16	0.87	3.808E-02	4.462E-03	3.346E-03	0.173	0.439	0.388	
11.65	1.05	0.9	4.481E-02	4.038E-03	3.462E-03	0.189	0.442	0.368	

*Saturation trajectory

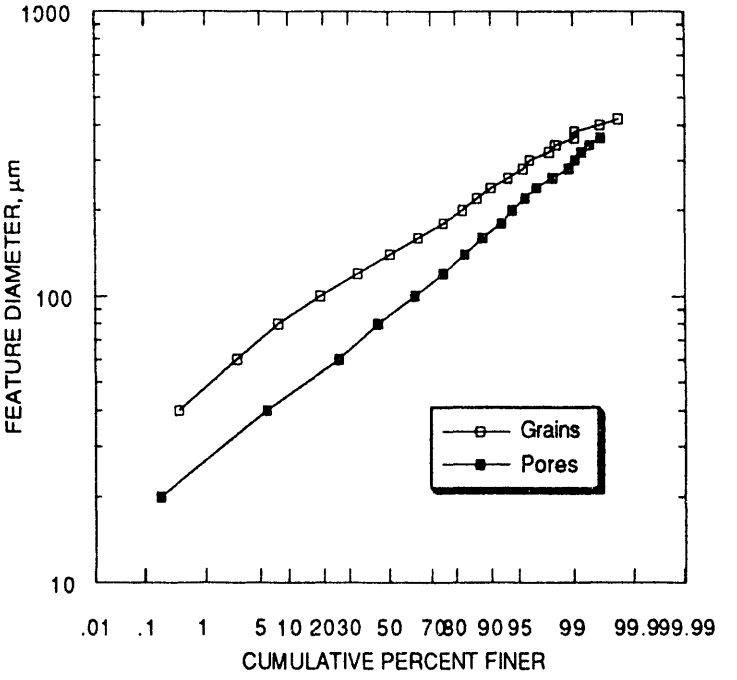

FIGURE 1. - Grain and pore diameter distributions from thin-section analyses, fired 260-mD Berea sandstone.

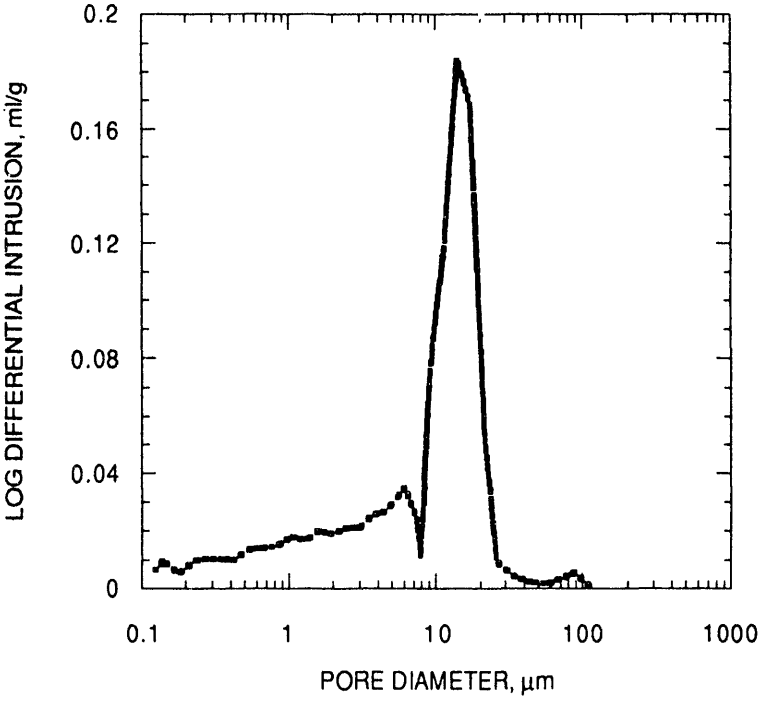

FIGURE 2. - Mercury intrusion porosimetry results, fired 260-mD Berea sandstone.

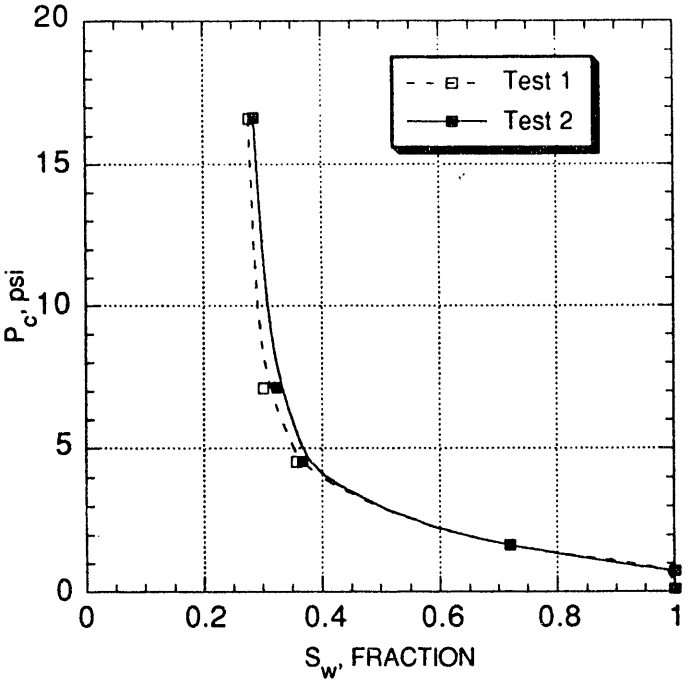

FIGURE 3. - Capillary pressure curves for two samples of 260-mD Berea.

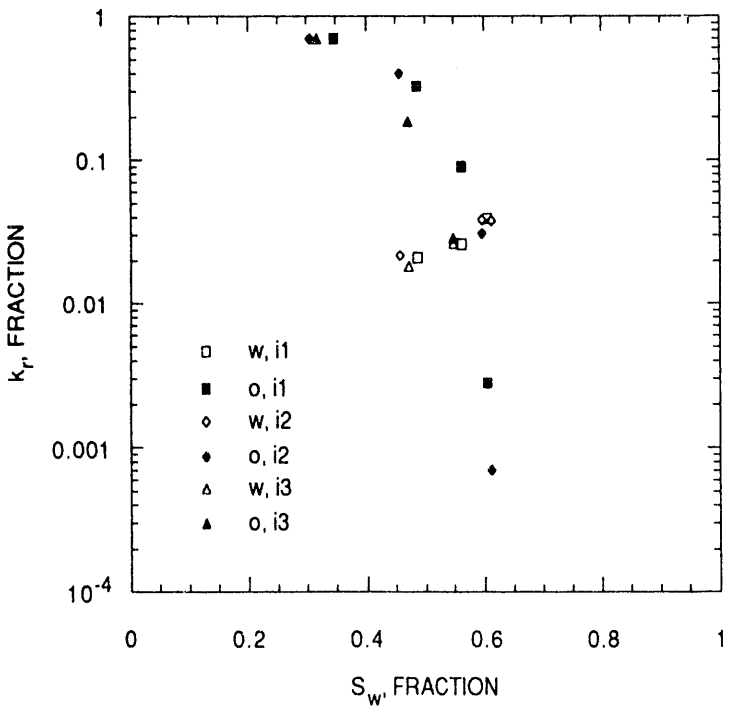

FIGURE 4. - Unsteady-state oil/water relative permeability results, fired Berea sandstone with 500 psig confining pressure. Data are normalized with respect to k_w = 157-mD at S_w = 1.0.

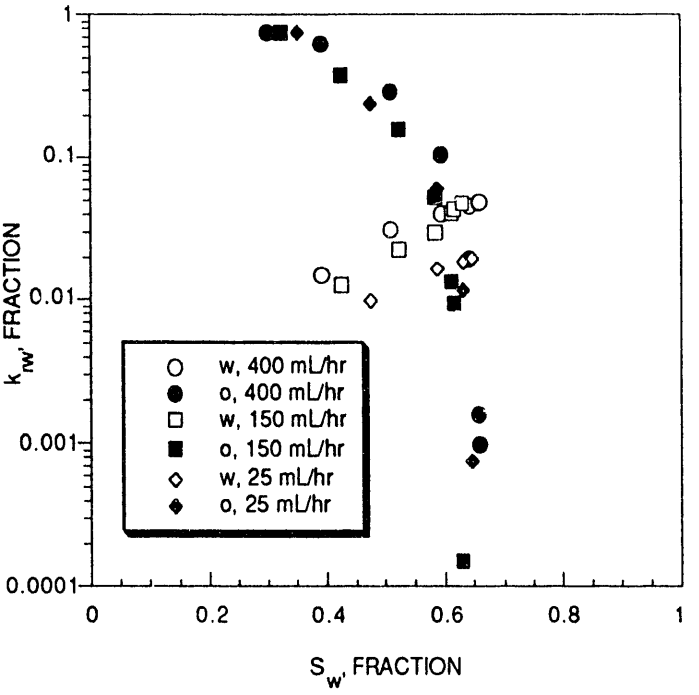

FIGURE 5. - Unsteady-state relative permeability results for 260-mD Berea sandstone with injection rates of 400, 150, and 25 mL/hr. The confining pressure was 500 psig.

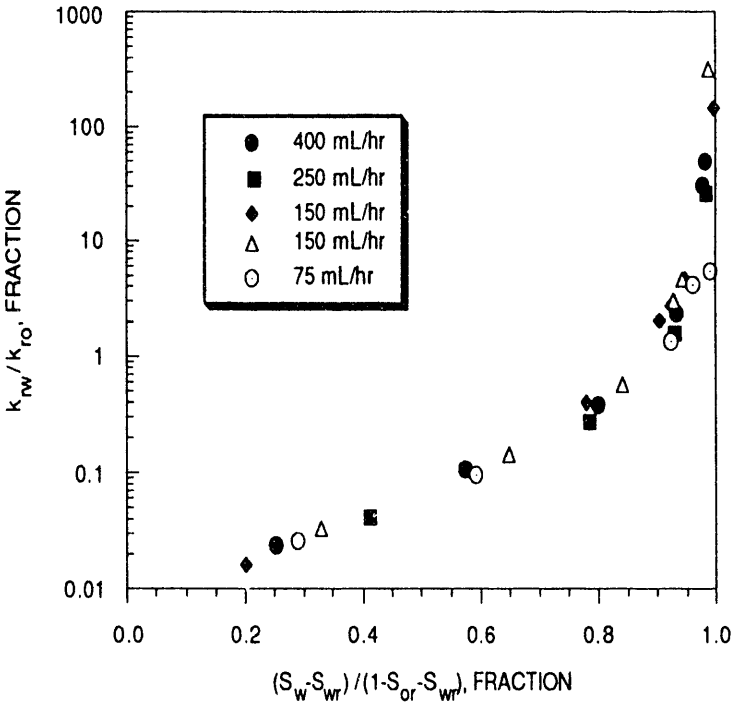

FIGURE 6. - Relative permeability ratio versus normalized saturation, 260-mD unsteady-state oil/water relative permeability test results.

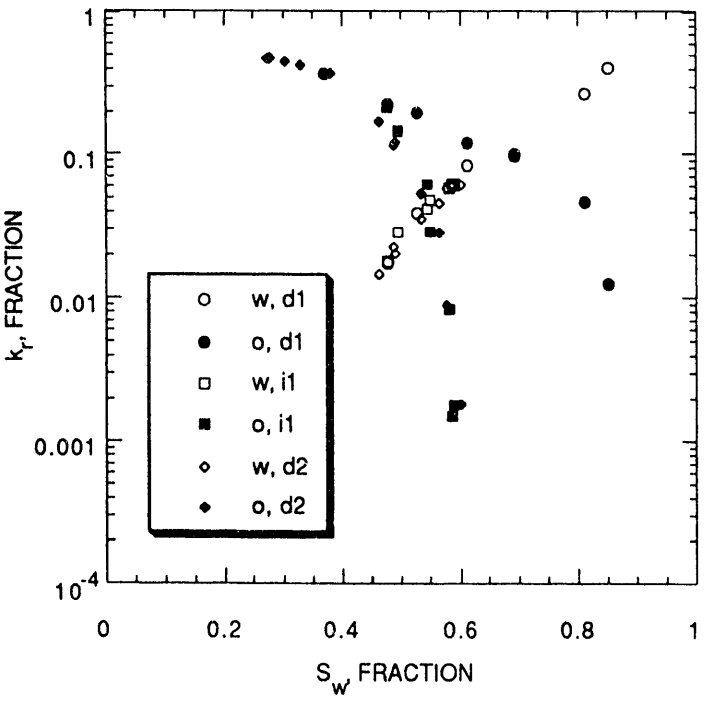

FIGURE 7. - Steady-state oil/water relative permeability results, Berea sandstone with 3,200 psig confining pressure. The data are normalized with respect to k_w = 260-mD at S_w = 1.0.

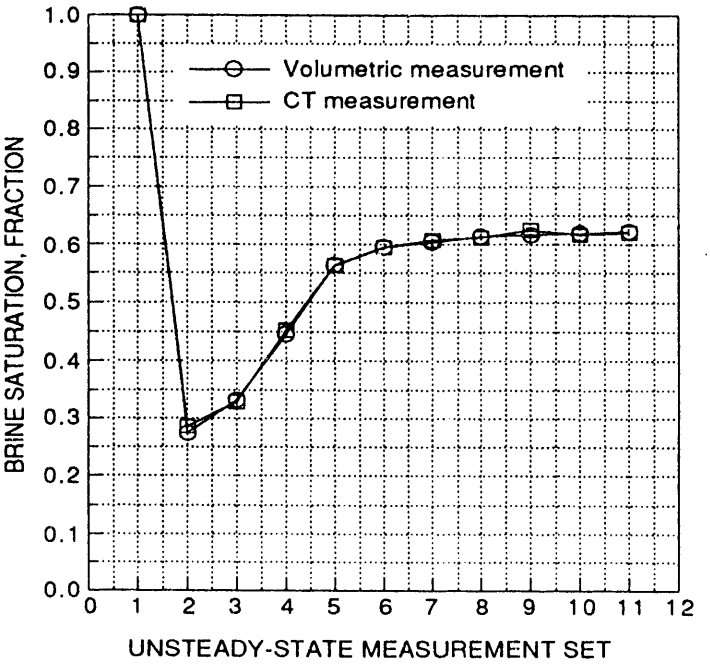

FIGURE 8. - Comparison of brine saturations determined by volumetric and CT techniques during the waterflood test.

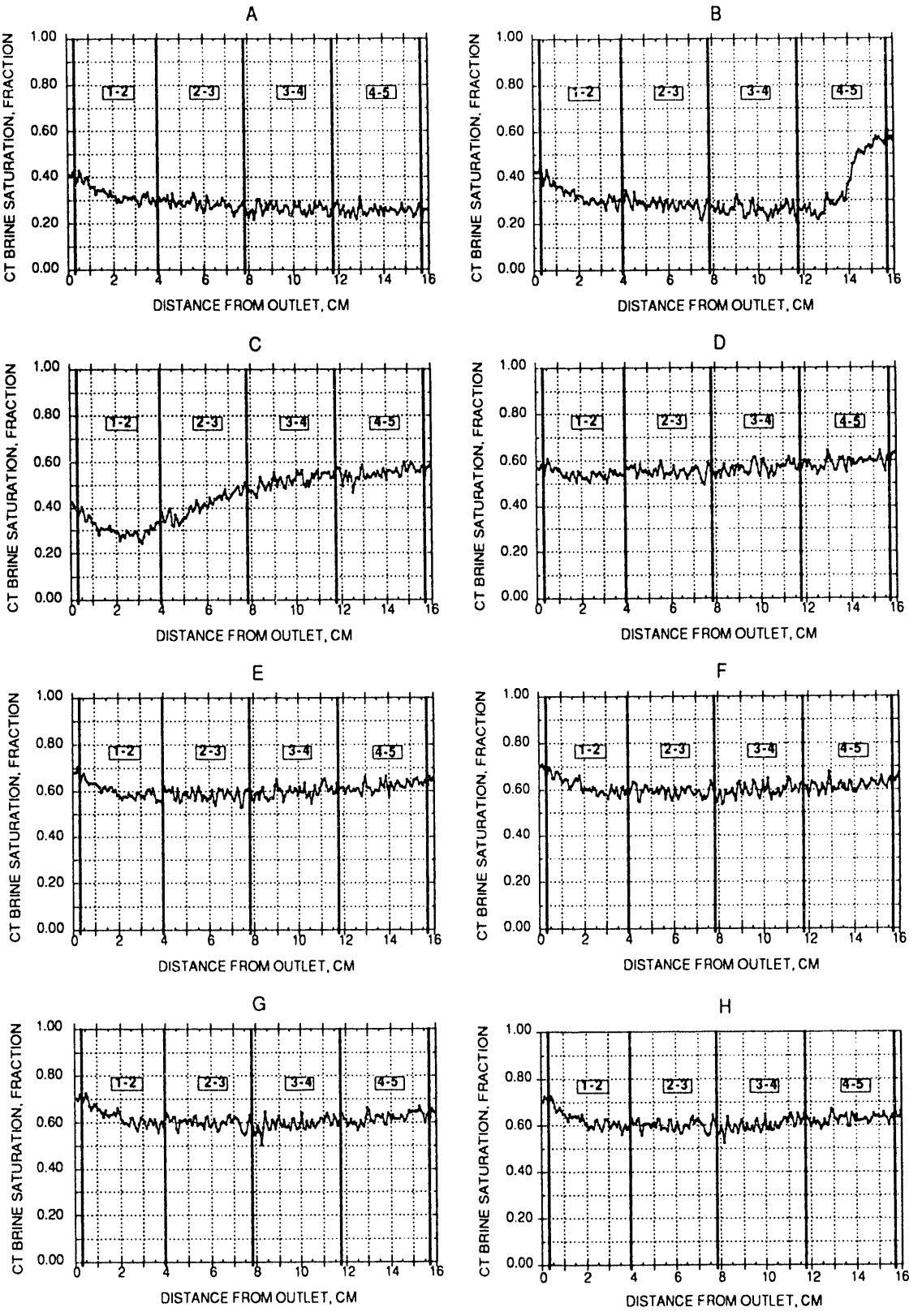

FIGURE 9. - Saturation distributions during the waterflood test from CT measurements. The heavy lines show the locations of the resistivity electrodes.

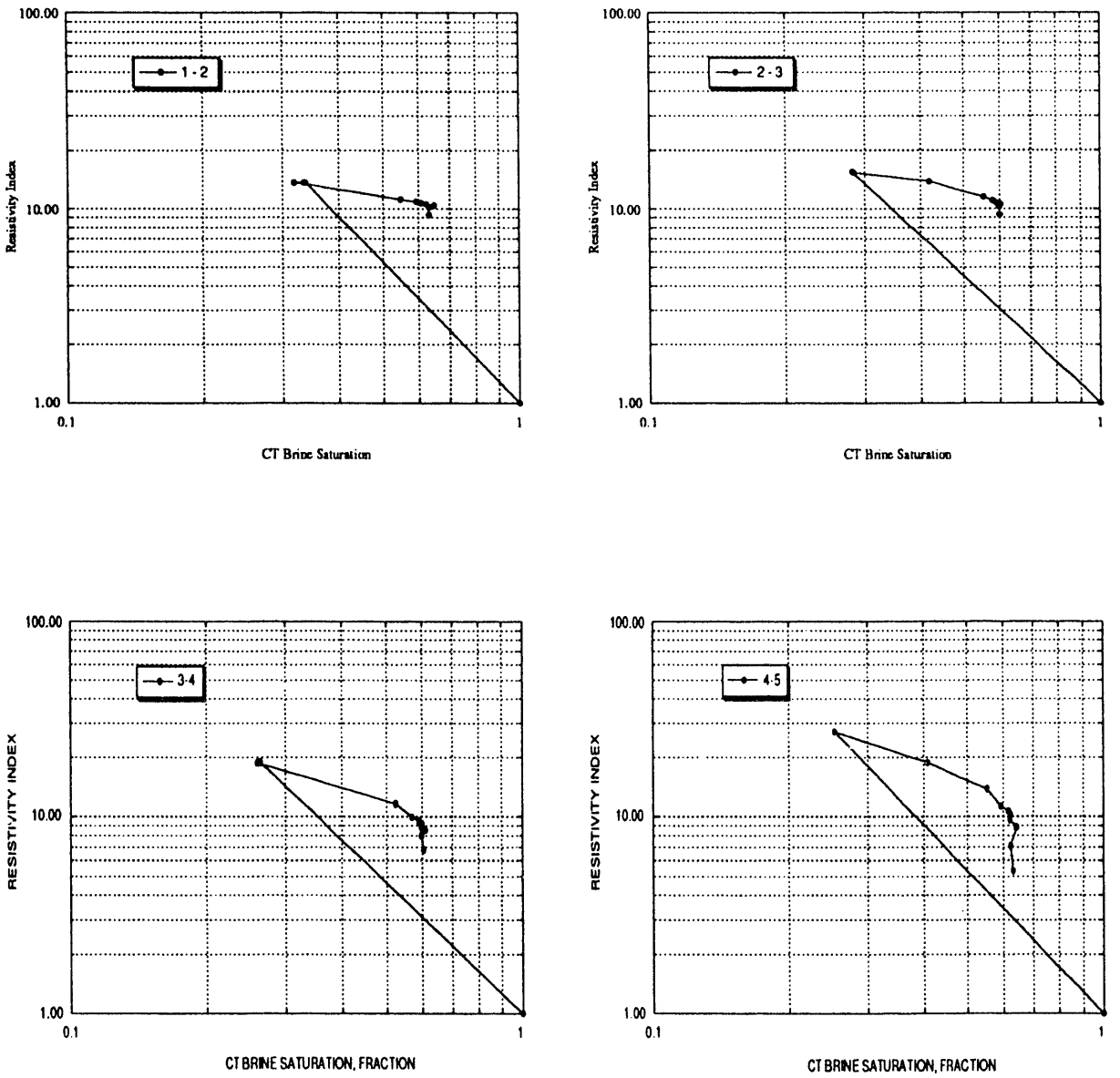

FIGURE 10. - Resistivity indices during the waterflood. The lines track the sequence of test measurements.

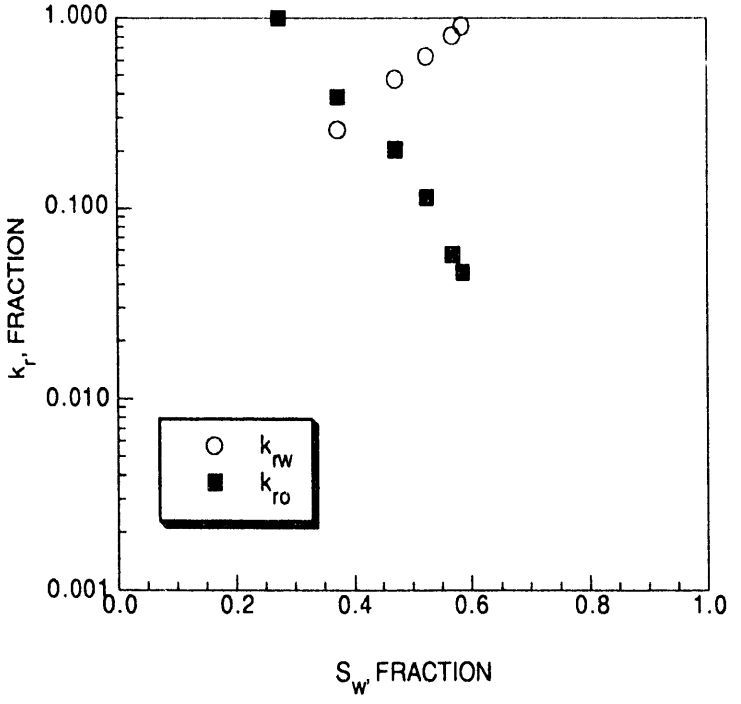

FIGURE 11. - Unsteady-state oil/water relative permeability results calculated from the CT/waterflood fluid production and pressure drop measurements.

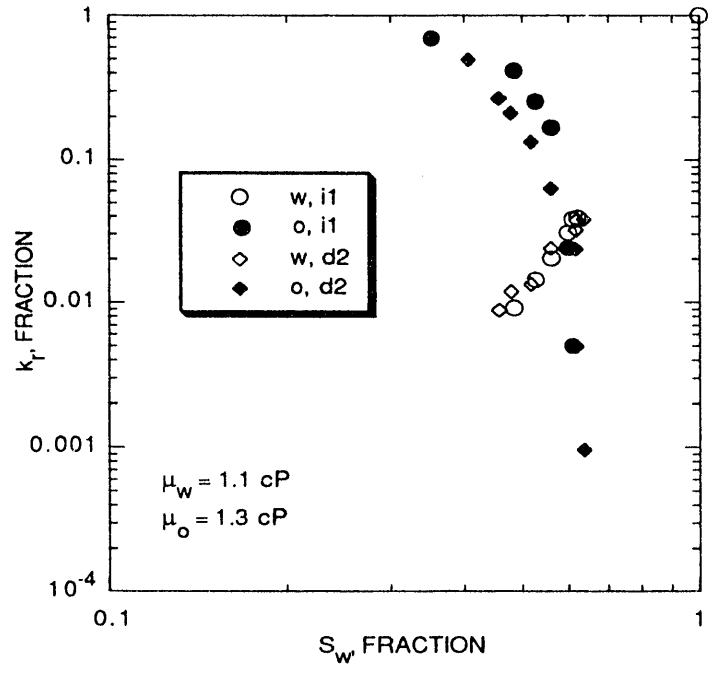

FIGURE 12. - Steady-state oil/brine relative permeability results. Normalized with respect to k_w = 260-mD when S_w = 1.0.

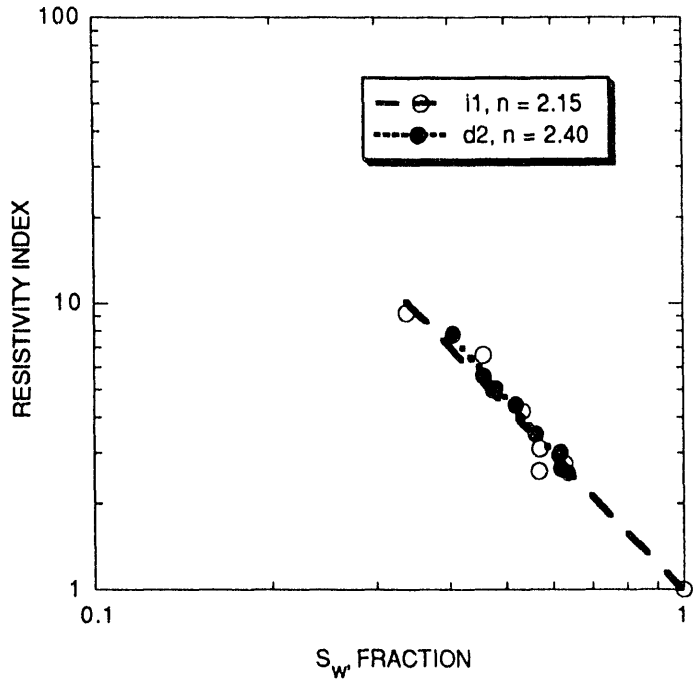

FIGURE 13. - Resistivity results from the oil/brine steady-state test, 260 mD Berea sandstone.

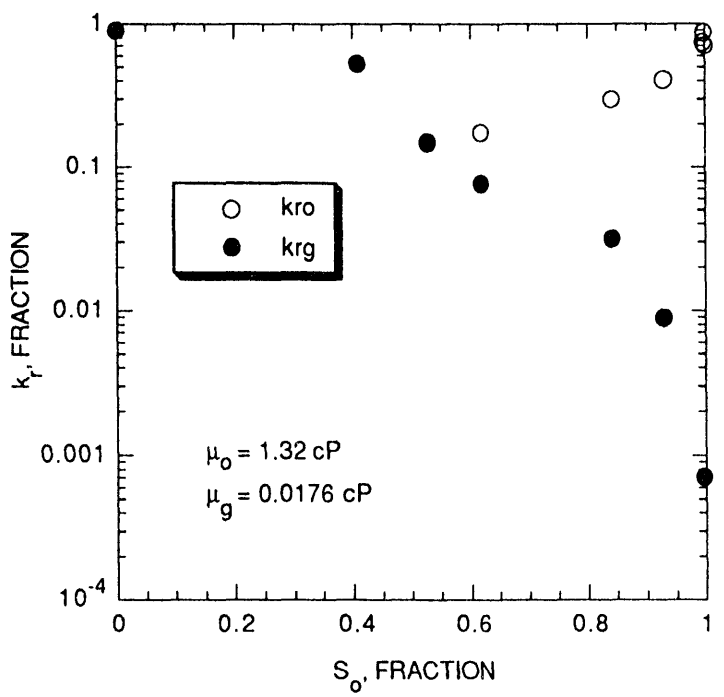

FIGURE 14. - Oil/gas relative permeability results. Normalized with respect to k_w = 260-mD when S_w = 1.000.

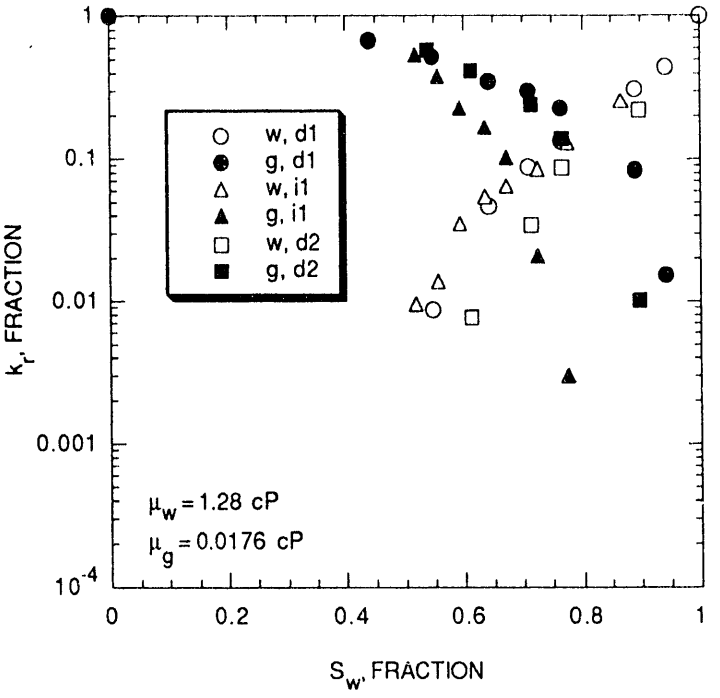

FIGURE 15. - Gas/water steady-state results. Normalized with respect to k_w = 260-mD at S_w = 1.0.

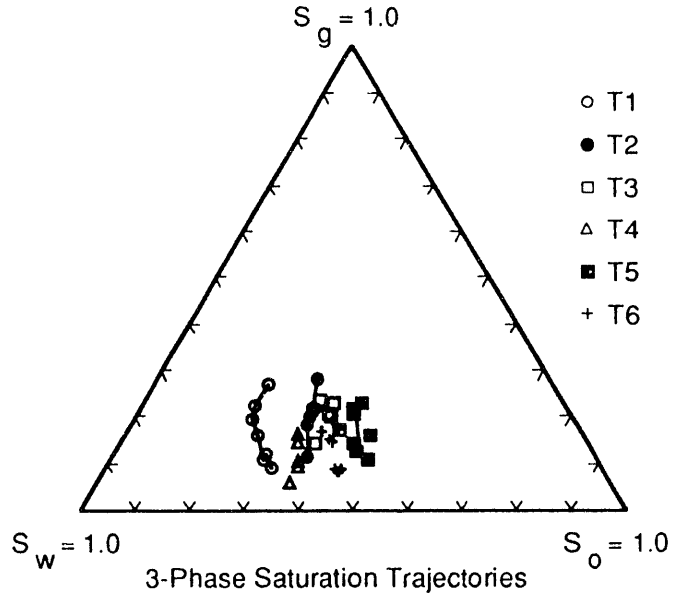

FIGURE 16. - DDI saturation trajectories during three-phase relative permeability measurements.

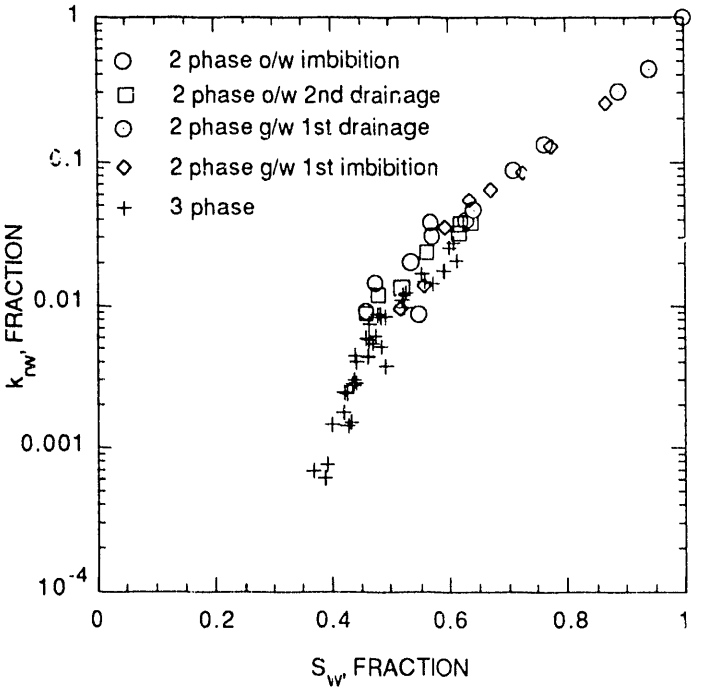

FIGURE 17. - Water relative permeability results from two- and three-phase measurements. The data are normalized with respect to k_w = 260-mD when S_w = 1.0.

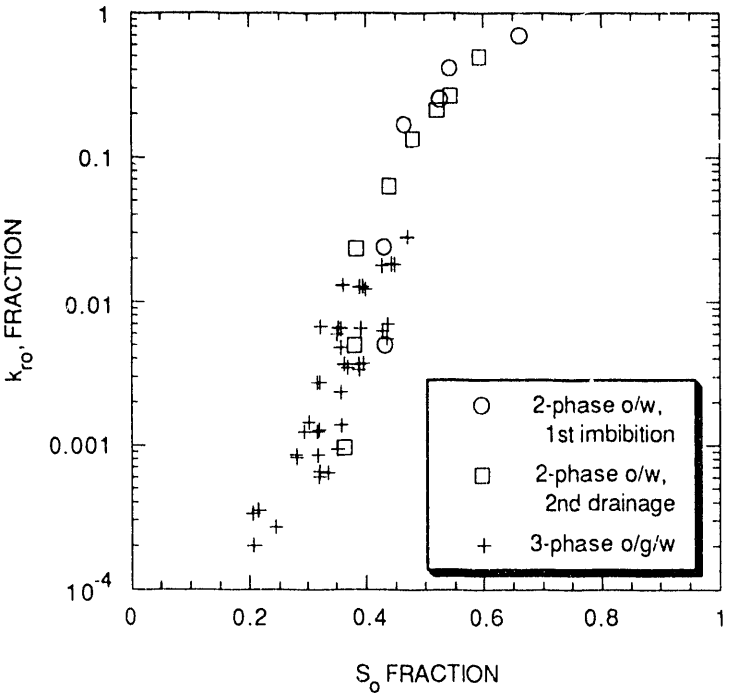

FIGURE 18. - Oil relative permeability results from two- and three-phase measurements. The data are normalized with respect to k_w = 260-mD when S_w = 1.0.

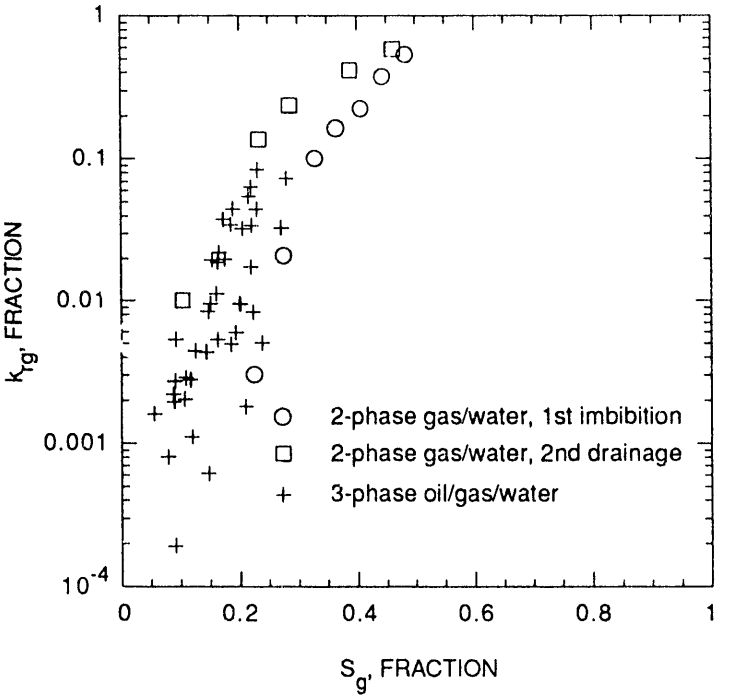

FIGURE 19. - Gas relative permeability results from two- and three-phase measurements. The data are normalized with respect to k_w = 260-mD when S_w = 1.0.

APPENDIX A

X-RAY AND MICROWAVE ATTENUATION TECHNIQUES FOR DETERMINING TWO- AND THREE-PHASE SATURATIONS

During steady-state tests, oil and water (brine) saturation distributions are measured in situ by X-ray and microwave attenuation techniques. For two-phase tests in which one of the fluid phases is water, the X-ray and microwave results are directly comparable and generally agree to within 3 saturation units (or to within 0.03 on a saturation scale from 0 to 1.0).

To conduct a scan, the X-ray or microwave instrument is advanced to the outlet face of the rock sample. An X-ray or microwave beam of 1 cm diameter (approx.) is directed at the center of the sample. The decrease in X-ray or microwave intensity is measured as the beam passes through the rock. After recording the measurements, the scanner is advanced 7 mm to the next scan position. Similar measurements are recorded until the instrument reaches the outlet face of the sample. The X-ray and microwave scans provide attenuation data representative of a plane through the center of the sample from the inlet to the outlet. Saturation distributions are calculated by the techniques described in the following paragraphs. The pressure taps that are used for ΔP measurements during the tests on plastic-encased rocks are spaced at least 2.5 cm away from the inlet and outlet faces of the rock so that capillary end effects do not influence the permeability measurements. The saturations between the pressure taps are averaged and these averages are plotted against relative permeabilities on the relative permeability graphs. Unique microwave and X-ray calibrations are determined for each rock and fluid system at the start of each test.

Figure A-1 shows a typical microwave calibration curve in which the natural log of the incident microwave power (a) divided by the emergent microwave power (b) is plotted against water saturation. The attenuation of the microwave signal is principally governed by the amount of water in the sample and calibrations are almost identical whether the second phase is oil or gas. For this reason, the microwave scanner is an excellent tool for measuring brine saturations during both two- and three-phase tests as long as the containment system does not reflect or absorb microwaves. Our low-power microwave klystron does not excite the water molecules sufficiently to cause a measurable increase in the temperature of the fluid system.

Figure A-2 shows typical X-ray calibrations in which the natural log of the emergent X-ray intensity [Ln(I)] is plotted against oil saturation. In our system, the incident X-ray intensity is assumed to remain constant and generally does, except immediately before the tube or some other component within the X-ray circuitry fails, causing an abnormal decrease in the emergent X-ray attenuation. Two calibrations are shown; one for an oil/water system and a second for an oil/gas system. A third calibration, which is not shown, can be constructed to calculate water saturations from X-ray measurements in a gas/water system. The calibrations are dependent on the volumes of each fluid present in the system. For a test in which only two fluid phases are present in the rock, the appropriate calibration is used to calculate the fluid saturations within the rock. In a three-phase system, water saturations are determined from microwave results while the oil saturation is determined by:

$$S_o = (S_o)_{ow} + \left(1 - \frac{S_w}{1-(S_o)_{ow}}\right)[(S_o)_{ow} - (S_o)_{og}] \quad \text{(A-1)}$$

Where S_O is the oil saturation, S_W is the water saturation from microwave results, $(S_O)_{OW}$ is the oil saturation calculated from the oil/water calibration equation, and $(S_O)_{OG}$ is the oil saturation calculated from the oil/gas calibration equation. The plane defined by the two lines on Fig. A-2 describes the combinations of X-ray scan results and oil saturations that may occur during a three-phase test. The slopes of the calibration lines depend upon the amount of X-ray tagging agent that is added to one of the fluid phases. Figure A-2 results are for a refined oil tagged with 10% by weight iodododecane. A higher tag concentration yields a lower Ln(I) value for the oil saturated rock, increasing the resolution of the saturation measurement.

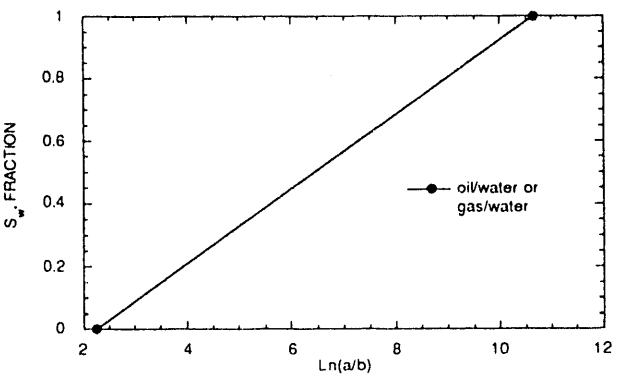

FIGURE A-1. - Typical microwave calibration for one position within the rock sample.

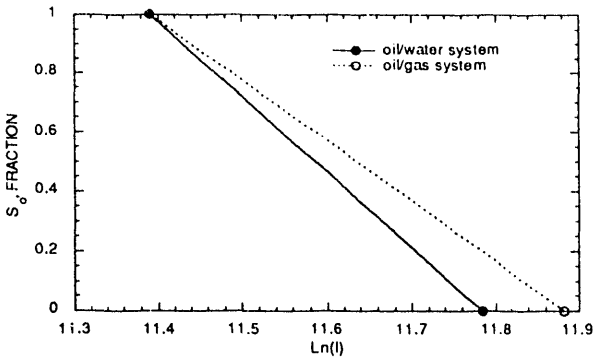

FIGURE A-2. - Typical oil saturation calibrations for one position within the rock sample.

For many tests, it is not desirable to completely saturate the rock with oil when generating X-ray calibration data. One method that we use to completely calibrate the X-ray is to scan the dry rock, then scan the brine saturated rock, and finally scan the rock when saturated with a brine that contains a tagging agent which identically matches the linear attenuation characteristics of the oil phase. The tagged brine can be flushed out of the system, leaving the rock completely saturated with brine and ready for the relative permeability test.

APPENDIX B

DUAL ENERGY X-RAY TECHNIQUES FOR MONITORING THREE-PHASE SATURATIONS

The current practice in the NIPER relative permeability laboratory is to use both X-ray and microwave scanners for three-phase saturation determinations. A literature study and evaluation of X-ray characteristics of materials were conducted during the project year to determine if the NIPER X-ray scanner could be operated in the 'dual energy ' mode, providing an additional check on the accuracy of the saturation measurements. The technique requires tagging both the brine and oil phases with X-ray tags of different attenuation characteristics.

Background

From chapter 2 of ref. 1, if a perfectly collinear monochromatic x-ray beam of intensity I_0 is directed at an absorber of thickness t and density ρ and X-ray masks are placed on both sides of the absorber, the emergent beam has an intensity I, which is less than I_0 because of the absorption or attenuation of the X-rays in passing through the absorber. The emergent intensity is given by:

$$dI/I = - \mu dt \qquad \text{(B-1)}$$

where μ is the linear absorption coefficient (cm^{-1}) and the negative sign indicates that the intensity decreases upon passing through matter. Assuming μ is independent of thickness t (cm) yields the Lambert law:

$$I = I_0 e^{(-\mu t)} \qquad \text{(B-2)}$$

Two of the more useful X-ray absorption coefficients are the linear absorption coefficient μ and the mass absorption coefficient μ_m, which equals μ/ρ. Tables of μ_m versus X-ray wavelength can be found in the literature. Taking advantage of the relationship between X-ray wavelength (w) and excitation potential (V, KV)

$$w = 12.396/V \qquad \text{(B-3)}$$

allows one to calculate mass attenuation coefficients for various elements at different X-ray potentials.

Attenuation coefficients generally increase with decreasing wavelength. However, abrupt discontinuities known as absorption edges or critical absorption wavelengths occur which are significant. The best tags for X-ray saturation determination are materials containing an element for which a critical absorption edge occurs at a wavelength that is slightly longer than that of the test. The mass absorption coefficient for a mixture of elements can be calculated by

$$(\mu/\rho)_{AB} = (\mu_m)_{AB} = W_A(\mu/\rho)_A + W_B(\mu/\rho)_B \qquad \text{(B-4)}$$

where W_A is weight fraction A. Then the attenuation caused by a thickness of a mixture of elements can then be found from

$$I = I_0 e^{[-(\mu_m)_{AB}(\rho_{AB})t]} \qquad \text{(B-5)}$$

if the density of the mixture is known. Otherwise, the attenuation can be calculated from

$$I = I_0 e^{[-(\mu_m)_A(\rho_A)t_A]} \{e^{[-(\mu_m)_B(\rho_B)t_B]}\} \qquad \text{(B-6)}$$

A number of other factors influence X-ray attenuation, such as the distances between the X-ray source, absorber, and detector, type of detector used, and polychromatic nature of the X-ray beam. Because of these factors, one should consider that in practice, X-ray attenuation results will be somewhat different from calculations or predicted results using Eq. B-6.

Dual Energy Technique

Laird and Putnam[2] described a technique for determining three-phase saturations using cadmium chloride as an X-ray tag for the brine phase and iodobenzene as the X-ray tag for the oil phase in an oil-brine-gas three-phase system. A study was conducted to evaluate less hazardous tags. Mass attenuation coefficients for a number of candidate X-ray tags were calculated for a number of common tag/fluid combinations using Eq. B-4 and K spectrum data from appendix 7A from ref. 1 and from fluid densities measured in the laboratory. Potentials were calculated from wavelengths in appendix 7A of ref. 1 and using equation B-3. The results indicated that potassium bromide and iododecane might be adequate for tagging the brine and oil phases in a three-phase system. The potassium bromide and iododecane tag concentrations can be selected such that the two fluids will have identical attenuation characteristics at one X-ray energy and different attenuation characteristics at a second energy. Table B-1 shows calculated linear

attenuation characteristics for nitrogen gas, 3.406% by weight KBr in water, and 16% by weight iododecane in decane at potentials of 24.792 KV (25 KV is the lower limit on the NIPER machine) and 41.320 KV at ambient conditions.

Note that the linear attenuation coefficient for nitrogen gas is very low but non-zero. As the linear attenuation coefficient is sensitive to density, changes in temperature and pressure that affect the fluid densities will also affect their linear attenuation coefficients.

The X-ray results at both potentials were calculated assuming various three-phase saturation conditions. For simplicity, equation B-6 was rewritten as

$$T = I/I_0 = e^{-(\mu_g t_g)} \times e^{-(\mu_w t_w)} \times e^{-(\mu_o t_o)} \qquad \text{(B-7)}$$

where T is the transmission factor (adopted from Laird and Putnam) and subscripts g, w, and o denote gas water and oil. Assuming that the X-ray beam passes through a unit thickness containing gas, oil, and water, transmission factors for various saturation conditions were calculated by assuming that each phase could be modeled as a thickness of fluid. Calculations were found to be simplified when -Ln(T) was used rather than T. Figure B-1 graphically shows some of the results at 24.79 KV and 41.32 KV potentials. Since the attenuation characteristics of the water and oil phases were made equal at the 24.79 KV potential, the gas saturation can be easily calculated at the 24.79 KV condition regardless of oil and water saturation. Once the gas saturation is known, the oil and water saturations can be calculated from the 41.32 KV results.

This evaluation of dual energy X-ray techniques indicates that the linear X-ray scanner in the NIPER relative permeability lab may be sufficient to take advantage of this technology to improve the accuracy and reliability of the three-phase saturation measurements if X-ray scans can be taken at two energy levels on both sides of the iodine K absorption edge.

In the previous example, the X-ray voltage settings of 24.7 and 41.3 KV were selected to provide intensity measurements on either side of the iodine K absorption edge which occurs with an excitation potential of 33.2 KV. Additional calculations were performed to evaluate the suitability of using the technique for potentials above the K absorption edges of the fluids. The calculations assumed

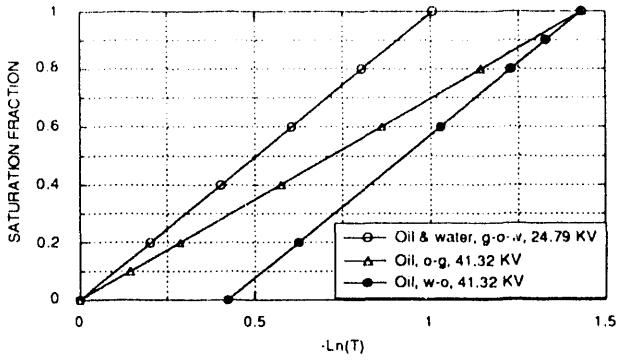

FIGURE B-1. - Saturation fraction versus -Ln(T) from example calculations.

that the oil phase consisted of decane tagged with iododecane while the brine phase consisted of KBr in water. Linear attenuation coefficients were calculated for the two fluids for potentials of 50 and 55 KV. The results are shown in Fig.B-2.

Assume that the two fluids are tagged to have linear attenuation coefficients equal to 0.5 cm^{-1} at the 50 KV potential. To achieve this condition, the oil phase is tagged with 8% by weight iododecane while the brine phase is tagged with 10% KBr. When the potential is stepped up to 55 KV, the oil phase linear attenuation coefficient is approximately 0.3. The brine phase linear attenuation coefficient is also about 0.3. As the attenuation coefficients for the two fluids are nearly identical at both X-ray potential settings, the tagging arrangement would not be very useful for measuring fluid saturations during three-phase tests. Reviewing the results of Fig. B-2, for practically any KBr/brine and iododecane/decane system in which the brine and oil phases are tagged to have similar X-ray attenuation coefficients at the 50 KV potential, the linear attenuation coefficients for the two fluids are also similar at the 55 KV potential. The best contrast in the attenuation characteristics of the two tagged fluids occurs when the X-ray operating potentials are within 5 to 10 KV on either side of a prominent absorption edge for one of the two fluids.

TABLE B-1. - Calculated linear attenuation coefficients at two potentials

	Linear attenuation coefficient, μ, cm^{-1}		
Potential, KV	Nitrogen	3.406% KBr in water	16% iododecane in decane
24.792	5.000×10^{-4}	1.006	1.006
41.320	2.500×10^{-4}	0.422	1.433

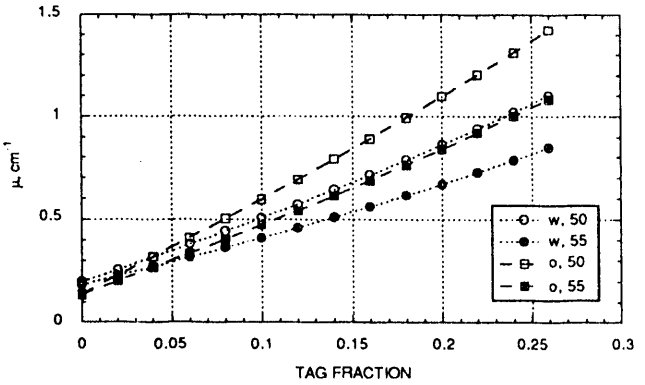

FIGURE B-2. - Linear X-ray attenuation coefficients for brine tagged with KBr (w) and decane tagged with iododecane at potentials of 50 and 55 KV.

References

1. Bertin, E. *Principles and Practice of X-Ray Spectrometric Analysis.* Second Edition. Plenum Press, New York, 1975.
2. Laird, A. and J. Putnam. Three-Component Saturation in Porous Media by X-ray Techniques. *Petroleum Transactions, AIME*, Vol. 216, 1959. pp. 216 - 220.

APPENDIX C

USING A WEIGHT METHOD FOR FLUID PRODUCTION MEASUREMENTS DURING UNSTEADY-STATE TESTS

The manner in which brine and oil production versus time data are recorded during an unsteady-state relative permeability test affects the accuracy of the results. Typical test measurements are obtained by recording the pressure drop across the length of the sample, and oil and brine volumes collected in a series of graduated collection flasks at several times during the test. Obtaining a number of good measurements immediately after water breakthough is critical and often very difficult depending on the nature of the test. Recording the fluid volumes in collection tubes can be tedious, especially when the brine and oil do not readily separate.

An automated method of recording fluid production volumes during unsteady-state tests is required. One choice would be to use a separator which is available on the market. The separator consists of two compartments: one in which the fluids enter and another connected compartment in which the position of the oil-water interface is established by a sonic technique. An alternative method for tests that do not require backpressure is to take advantage of the difference in fluid densities to monitor production. This report describes a system designed in our laboratory to continuously measure the cumulative weight of oil and cumulative weight of brine produced during an unsteady-state test. Fluid volumes are then calculated from the weight measurements. The system is well suited for oil/brine systems that exit the rock in the form of an emulsion since the oil and brine in the oil collection vessel do not have to be well segregated in order to calculate the produced fluid volumes.

Principle of Operation

Figure C-1 shows the proposed method for automating unsteady-state volume measurements. The apparatus consists of two collection vessels, U1 and U2. U1 is a closed vessel, initially filled completely with brine, with an inlet from which test fluids enter and an outlet from which one drop of brine flows for every drop of brine or oil that enter U1. Each drop of brine that leaves U1 is captured in U2. A film of oil on the surface of brine in U2 prevents the brine in U2 from evaporating. As long as the densities of the brine and oil test fluids are constant and the load cells used for weight measurements are accurate, the produced fluid volumes can be calculated at any time during the test from the change in U1 and U2 weights as described in the following calculations.

V_o = oil volume, cm^3
V_w = water volume, cm^3

ρ_o = oil density, g/cm^3
ρ_w = water density, g/cm^3
$\Delta U1$ = weight change for U1, g (compared to initial weight)
$\Delta U2$ = weight change for U2, g (compared to initial weight)

Since the total volume of U1 is constant,

$$\Delta U1 = \Delta V_o(\rho_o - \rho_w) \quad \text{(C-1)}$$

$$\Delta U2 = (\Delta V_o + \Delta V_w)\rho_w \quad \text{(C-2)}$$

From Eq. C-1 and C-2,

$$\Delta V_o = \Delta U1/(\rho_o - \rho_w) \quad \text{(C-3)}$$

$$\Delta V_w = [\Delta U2/\rho_w] - [\Delta U1/(\rho_o - \rho_w)] \quad \text{(C-4)}$$

Typical Application

For a typical unsteady-state relative permeability test, the oil and brine densities are about 0.86 g/cm^3 and 1.00 g/cm^3 respectively, for a density difference of 0.14 g/cm^3. Assuming the required measurement resolution is to the nearest 0.1 cm^3, the weight accuracies required for the test are:

$\Delta U1 = (0.1\ cm^3)(-0.14\ g/cm^3) = -0.01\ g/0.10\ cm^3$ oil
$\Delta U2 = (0.1\ cm^3)(1.00\ g/cm^3)$
$= 0.10\ g/0.10\ cm^3$ brine or oil

A typical plug might have the following characteristics:

L	=	7.62 cm
d	=	3.81 cm
A	=	11.4 cm
BV	=	86.9 cm
Ø	=	0.25
PV	=	21.7 cm

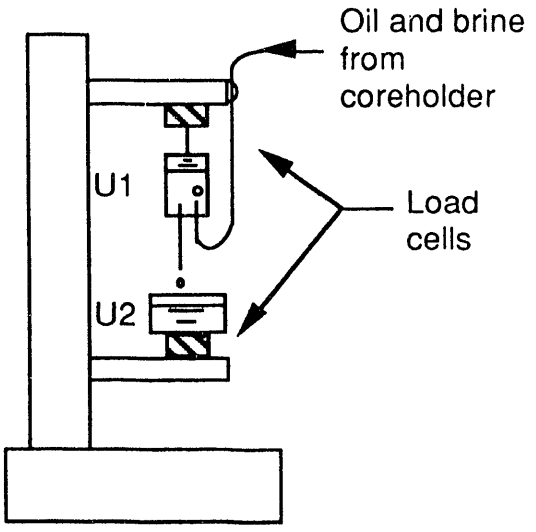

FIGURE C-1. - Proposed fixture for measuring unsteady-state fluid volumes.

Assuming S_{wr} is 0.3 and S_{or} is 0.7, the volume of oil that would be recovered during an unsteady-state relative permeability test would be approximately 9 cm^3. Therefore, U1 would require a volume of at least 9 cm^3. A 50 mL capacity would probably be sufficient for U1. If the U1 container weighed 30 grams and was initially filled with brine, the device used to measure U1 weight changes would require 100 gram capacity. If 20 pore volumes of fluid are injected during the test, U2 would require a volume capacity of approximately 420 cm^3. The device used to measure changes in U2 weight should have 500 gram capacity.

Demonstration Test for Proof of Concept

A demonstration test was conducted to verify the method of using weight measurements to monitor fluid production. An apparatus was assembled in a fashion similar to that of Fig. C-1 except that two Mettler digital balances were used for the weight measurements instead of load cells. A bottle arrangement like that shown for U1 in Fig. C-1 was suspended from the hook below the upper balance (Mettler PE 600) while a beaker was placed on the lower balance to capture effluent from the bottle. A syringe was used to push fluids into the bottle. The syringe was probably accurate to ± 0.1 mL. For every drop of fluid that entered the bottle, a drop left the bottle and fell into the beaker (U2). A film of oil was placed over the fluid in the beaker to prevent evaporation.

Two tests were conducted. The first test consisted of pushing brine only into the bottle, while the second test was conducted by pushing oil only into the bottle. Test results are provided in Table C-1. The results verify that the method should work well as long as the fluid densities are constant.

Discussion

Each unsteady-state test takes about 1 day to perform. When volumetric measurements are manually recorded from observing the fluid volumes in graduated cylinders and other vessels, the test operator must stay with the experiment from start to finish. Water breakthrough must be observed and accurately recorded (time, volumes). The work, although very important, is tedious.

The weight method described in this report is well suited toward experiment automation. Using electronic load cells for the weight measurements, an electronic ΔP transducer, and a controllable pump, the operator can delegate the responsibility of recording all of the test data from start to finish to a computer. The computer can take more measurements, is faster, and never gets bored or tired. The computer can also calculate the final results as the test progresses. The automated system is estimated to cost less than $4,000 and will save about 1 man-day of work per unsteady-state test. It is easy to imagine that the system can pay for itself in manpower savings. An alternative scheme which might work equally as well or better would be to use one load cell to monitor the combined weights of U1 and U2 while a second load cell monitors the change in weight of U1 or U2 separately, which might yield better resolution in volumetric calculations.

TABLE C-1. - Verification test results.

$\rho_o = 0.8386$ g/cm^3

$\rho_w = 1.078$ g/cm^3

$\rho_o - \rho_w = -0.2394$ g/cm^3

Injected volumes						Calculated volumes	
Vw, mL	Vo, mL	U1, g	U2, g	$U1/(\rho_o - \rho_w)$	$U2/\rho_w$	ΔVw, mL	ΔVo, mL
0.0	0.0	0.00	0.00	0.0	0.0	0.0	0.0
5.0	0.0	0.00	5.62	0.0	5.2	5.2	0.0
10.0	0.0	-0.01	10.73	0.0	10.0	10.0	0.0
15.0	0.0	-0.01	15.97	0.0	14.8	14.8	0.0
20.0	0.0	-0.01	21.42	0.0	19.9	19.9	0.0
0.0	0.0	0.00	0.00	0.0	0.0	0.0	0.0
0.0	5.0	-1.19	5.36	5.0	5.0	0.0	5.0
0.0	10.0	-2.40	10.89	10.0	10.1	0.1	10.0

*U.S.GPO:1992-661-026/60015

END

DATE
FILMED
6/15/92